Technische Universität München
Fakultät für Maschinenwesen
Professur für Biomechanik

# Material properties of bacterial biofilms

# Stefan Grumbein

Vollständiger Abdruck der von der Fakultät für Maschinenwesen der
Technischen Universität München
zur Erlangung des akademischen Grades eines

Doktor-Ingenieurs (Dr.-Ing.)

genehmigten Dissertation.

Vorsitzender: Univ.-Prof. Dr. Dirk Weuster-Botz
Prüfer der Dissertation:

1. Univ.-Prof. Dr. Oliver Lieleg
2. Univ.-Prof. Dr. Christian Große
3. Univ.-Prof. Dr. Andreas Bausch

Die Dissertation wurde am 31.03.2016 bei der Technischen Universität München eingereicht
und durch die Fakultät für Maschinenwesen am 18.07.2016 angenommen.

# Summary

Biofilms constitute a major problem in health care and industry where they can colonize catheters or plug pipes. The cost and time needed for removing and controlling those biofilms is immense. Therefore, finding new control and removal strategies has become a major part of biofilm research in the past. To develop such strategies, information about the material properties of bacterial biofilms is critically needed. However, measurements of material properties of biofilms are sparse, and it remains elusive how the molecular composition of the biofilm matrix affects the material properties of the bulk material. In this thesis, various material properties of two biofilms formed by different *Bacillus subtilis* (*B. subtilis*) strains are investigated and compared. In addition, specific biofilm components are identified which dictate selected material properties.

In the first part of this thesis, the erosion stability of biofilms formed by *B. subtilis* B-1 is determined. When these biofilms are exposed to shear flow established by fluids containing $Na^+$, $K^+$, or $Mg^{2+}$ ions, a linear increase in erosion with time is observed. However, other metal ions, *i.e.* $Ca^{2+}$, $Cu^{2+}$, $Zn^{2+}$, $Fe^{2+}$, $Fe^{3+}$, and $Al^{3+}$, are absorbed by the biofilm matrix and induce a protection against shear forces in this fluid flow. This protection from erosion is often accompanied by a mechanical fortification of the biofilm matrix which is quantified by macrorheology. Interestingly, many of those metal ions are toxic for planktonic *B. subtilis* B-1 bacteria, but the biofilm matrix shields the embedded bacteria by sequestering these metal ions. Furthermore, the chelating agent EDTA is able to remove some of those tested metal ions from the biofilm matrix, which, in turn, renders the biofilms sensitive to erosion again.

In the second part of this thesis, a stretching device is designed and assembled that allows for tensile testing of bacterial biofilms *in situ*. The design integrates key principles known from commercially available testing equipment, but uses a horizontal setup alignment to enable the treatment of biofilms directly in the measuring setup. A force curve can be extracted from the measured signal, which is then used to calculate the tensile strength and rupture energy of biofilms. When biofilms are treated with metal ions, and then are submitted to tensile forces in the custom-built elongational rheometer, a similar mechanical stiffening increase as already determined for the shear stiffness of biofilms is observed. Furthermore, the rupture energy of biofilms depends on the force loading rate which is typical for a network of transiently cross-linked polymers.

In the third part, further material properties of biofilms, *e.g.* their surface roughness, surface stiffness, and viscoelastic response, are determined and compared for biofilms formed by the two ge-

netically similar *B. subtilis* wild-type strains B-1 and NCIB 3610. In addition, three knock-out mutants of the strain NCIB 3610 are used to determine the influence of specific biofilm components on the bulk properties of the biofilm matrix. The surface layer protein BslA of the NCIB 3610 biofilm matrix is responsible for the surface stiffness and surface roughness of those biofilms, whereas the polyanionic γ-polyglutamate (γ-PGA), the main constituent of the B-1 biofilm matrix, is observed to prevent changes in the biofilm shear stiffness that arise from ethanol treatment of biofilms.

In the last part, it is shown that the addition of NCIB 3610 biofilms to standard mortar during the sample generation process stimulates the mineralization procedure during the hydration reaction of the mortar. As a consequence, the surface roughness is drastically increased for hybrid mortar samples, leading to an increased wetting resistance and a prevention of water uptake by capillary forces. When biofilms are lyophilized prior to the mixing process, higher amounts of biofilm powder can be added to the hybrid mortar mix, resulting in an even more pronounced wetting resistance. This hybrid material, generated from a biological material and the inorganic material mortar, shows a strong potential for industrial applications.

# Contents

# Introduction

Bacteria embed themselves in a matrix of self-produced biopolymers which is referred to as a bacterial biofilm. Biofilms are considered the most abundant and ubiquitous life form of bacteria since biofilms offer protection for the embedded bacterial cells from environmental hazards (1). The biofilm matrix is composed of a variety of different biomolecules, including polysaccharides, proteins, nucleic acids and lipids (2–5). These constituents are referred to as extracellular polymeric substances (EPS) and allow biofilms to resist wetting by liquids (6), protect residing bacteria from antibiotics and desiccation (7, 8), and absorb toxic metal ions without compromising the viability of embedded bacteria (9, 10). Biofilms can grow on a variety of different surfaces and are found in the most challenging environments, *e.g.* hot-springs (11), deep-sea vents (12), oil fields (13), or tooth surfaces (14). This extraordinary resilience of biofilms, however, can cause severe problems in health care and industry, where biofilms are able to colonize urinary catheters (15), reside in drinking water systems (16), and lead to plugging and corrosion of pipes (17). Removal of biofilms from pipes or - if this first strategy fails - a chemical inactivation generates enormous costs and is a time-consuming and difficult task (18, 19).

As a consequence, a lot of effort is put into the development of control and removal strategies for biofilms (20–22). However, such removal strategies critically depend on our understanding of which biofilm parameters prevent or promote biofilm growth. Whereas the chemical composition of many biofilm matrices has been identified (23), much less is known on how the different macromolecules in the biofilm matrix contribute to the complex material properties of biofilms (24, 25). Investigations on the role of particular matrix elements are challenging since the individual components of the EPS may have a multifunctional role in the biofilm matrix: for instance, alginate, a compound of the *Pseudomonas aeruginosa* biofilm matrix, is responsible for sequestering metal ions (9), providing structural integrity (26) and binding water (27). Additionally, suitable characterization methods to obtain information on the material properties of biofilms are sparse. Although the characterization of artificial materials is mostly standardized and a variety of test equipment is commercially available, the testing of biological samples is often not compatible with existing standard setups. A main challenge is measuring the low forces occurring in soft biological samples. Furthermore, the fixation and transfer of those soft samples may already alter or destroy the delicate biological material: a transfer of biofilm from its growth environment may easily alter the complex microarchitecture of the biofilm thus preventing the determination of the 'true' properties of the material (17). The need for a defined growth environment, together with the soft and sticky nature of the biofilm material also renders the casting of
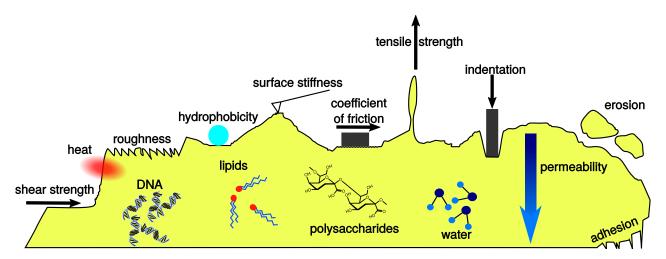
Figure 1.1: **Schematic illustration of a bacterial biofilm:** Biofilms are composed of various components including polysaccharides, proteins, lipids and DNA. A list of material parameters investigated in biofilm research is depicted together with pictographs representing different testing techniques.

biofilms into standardized test specimens, as needed for commercially available test equipment, very difficult. And on top of that, the extremely high water content of biofilms limits the use of techniques where samples need to be dried prior to examination, *e.g.* scanning electron microscopy (SEM), since drying could again alter the complex microarchitecture of the biofilms (28).

Nevertheless, the determination of material properties of biofilms and gaining a detailed understanding of how specific matrix components constitute and alter these properties is crucial for the development of suitable biofilm removal and control strategies. However, as typical in materials research, a broad range of parameters can be determined and used for comparing different biofilms. The schematic illustration in Figure 1.1 lists some examples of such materials parameters but - of course - is far from being complete. All those parameters listed play an important role for the biofilm behavior. The shear strength, adhesion, cohesion and erosion stability represent parameters that are relevant for scenarios which are found in *e.g.* pipes, where biofilms are exposed to liquid flow. Knowledge of these properties makes it possible to estimate how much flow is needed to remove biofilms in pipes. Information on the hydrophobicity and permeability of biofilms can be used to determine how chemicals and antibiotics might interact with the biofilm matrix and if they are able to penetrate the biofilm matrix to reach and kill the embedded bacteria. However, although biofilms are mostly undesired in industrial settings, some of the interesting material properties of biofilms are useful for technical applications. Examples of such technical applications of biofilms are wastewater treatment (29), the remediation of heavy metal-contaminated soil (30), or the industrial production of enzymes (31). These examples highlight the importance of biofilm research.

In this thesis, biofilms formed by the organism *Bacillus subtilis* (*B. subtilis*) are investigated as they serve as an established model system for biofilm formation (13, 32). In a first step, the erosion resistance of biofilms formed by the *B. subtilis* strain B-1 is determined in different chemical environments. Although, metal ions are potentially toxic for planktonic *B. subtilis* B-1, the biofilm matrix manages to

shield the embedded biofilm bacteria from this chemical hazard. The metal ions are sequestered by the biofilm matrix and protect those biofilms from erosion by shear forces. This mechanical protection is often accompanied by an increase in the shear stiffness of the biofilm matrix. A similar biofilm stiffening after exposure to metal ions is also observed when those biofilms are submitted to tensile forces in a custom-built elongational rheometer. The design of this stretching device is discussed and measurements of the tensile strength and the rupture energy of *in situ* grown biofilms are presented. In a further step, various material properties, *e.g.* the surface roughness, surface stiffness, and viscoelasticity of *B. subtilis* B-1 biofilms, are determined and compared to biofilms formed by another *B. subtilis* strain (NCIB 3610) and selected knock-out mutants of this strain. Variations in the matrix composition of these biofilms are found to be responsible for differences in the biofilm surface roughness and surface stiffness. γ-polyglutamate (γ-PGA), the main constituent of the B-1 biofilm matrix is shown to prevent shear stiffness changes arising from an ethanol treatment of B-1 biofilms. In turn, ethanol-sensitive NCIB 3610 biofilms can be supplemented with γ-PGA so that they gain the same protection effect from ethanol. In a last step, it is shown that the addition of NCIB 3610 biofilms to standard mortar during the sample generation process stimulates the mineralization process during the hydration reaction of mortar. Hence, the surface roughness is drastically increased for hybrid mortar samples, leading to an increased wetting resistance and a prevention of water uptake by capillary forces. This hybrid material, generated from a mixture of biological and inorganic components illustrates the strong potential of biofilms for industrial application and the need for a deeper understanding of biofilm properties in general.

# Materials & Methods

The following methods are mainly adopted from Grumbein *et. al*(10) and Kesel *et. al*(33).

## 2.1 Biofilm and sample preparation

### 2.1.1 Bacterial strains

Two bacterial wild-type strains *B. subtilis* B-1 (34) and *B. subtilis* NCIB 3610 (35) were used for the experiments. Additionally to these wild-type strains, mutants of the strain NCIB 3610 lacking specific matrix main components were used. These mutant strains were CA017, N24 and ZK3660, each of them is unable to produce one main matrix component. *B. subtilis* strain CA017 is unable to produce the TasA protein (36), whereas strain N24 is lacking production of the surface protein BslA (37). In strain ZK3660, the gene for exopolysaccharide EpsA-O (38) production was knocked out. An overview is given in Table 2.1.

### 2.1.2 Biofilm formation

The following two protocols for biofilm formation were used and are indicated for the experiments:
*Formation protocol F1:* Overnight cultures were grown from a frozen glycerol stock in liquid Lysogeny Broth (LB) (according to Luria/Miller) medium, and incubated at 37 °C and 90 rpm for 13 hours. Biofilms were grown by plating 100 µL of an overnight culture onto 1.5 % (w/v) agar plates containing LB and

| Strain | Description | Remaining matrix composition | | | Antibiotic [µg/mL] | Reference |
|---|---|---|---|---|---|---|
| | | TasA | BslA | EpsA-0 | | |
| NCIB 3610 | Wild-type | x | x | x | None | (35) |
| CA017 | TasA::Kan | | x | x | Kanamycin (50) | (36) |
| N24 | BslA::Cam | x | | x | Chloramphenicol (5) | (37) |
| ZK3660 | EpsA-O::Tet | x | x | | Tetracycline (12.5) | (38) |
| B-1 | Wild-type | Mainly γ-polyglutamate | | | None | (34) |

Table 2.1: Table of bacterial strains with the main matrix components and the corresponding antibiotic used for selecting the strains

incubating those agar plates at 37 °C for 24 hours.

*Formation protocol F2:* Bacteria were streaked out onto 1.5 % (w/v) agar plates containing LB and those agar plates were then incubated at 37 °C for 9 hours. A single colony was picked, grown in liquid LB medium and incubated at 37 °C and 300 rpm for 9 hours. Biofilms were grown by plating 210 µL of an overnight culture onto 1.5 % (w/v) agar plates containing LB and incubating those agar plates at 37 °C for 13 hours.

The corresponding antibiotic according to Table 2.1 was added to the liquid cultures during growth of the mutant strains. This ensured that only the desired mutant is able to grow and used for biofilm formation.

### 2.1.3 Biofilm treatment

Fresh biofilm was prepared according to the protocols established above and treated with different solutions to study the effect of those solutions on the biofilm properties. The treatment was performed prior to the experiments according to one of the following protocols.

*Treatment protocol T1:* Biofilm was carefully scraped from the agar with a glass slide without damaging the underlying agar surface. The biofilm material was then pooled, split into small amounts (~500 mg), transferred into micro test tubes and weighed. 5 % (v/w) of a chemical stock solution was then added to the tubes and the chemical was distributed throughout the biofilm by gentle stirring with a pipette tip. Treated biofilm samples were kept at room temperature for 1 hour prior to their characterization.

*Treatment protocol T2:* Biofilm was fully covered with a chemical stock solution. After defined time intervals, the solution was disposed and the biofilm samples were kept at room temperature for 10 minutes to allow for evaporation of the remaining solution prior to characterization.

It will be indicated throughout the thesis which protocol was used for each experiment.

### 2.1.4 Sample preparation for elongational rheology

For this purpose, LB was dissolved in double-distilled water (ddH$_2$O) and enriched with 1.5 % (w/v) agar. The autoclaved, still liquid LB-Agar was poured into the customized sample holder (Fig. 2.1) where it formed a continuous nutrition layer. After gelation of the agar, the solid layer was sliced at the touching points of the two sample holder parts using a sterile scalpel. Subsequently, a Drigalski spatula was used to spread 15 µL of the bacterial liquid culture (prepared as in protocol *F1*) of *B. subtilis* B-1 on the rectangular part of the agar layer. The sample holders were then placed in the incubator at 37 °C and incubated overnight. On the next day, a continuous biofilm layer was formed, and the samples could be used for mechanical testing. A more detailed description can be found in Section 3.2.1.
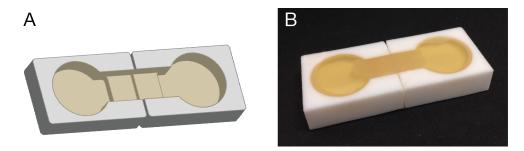
Figure 2.1: **Sample holder for elongational rheology experiments:** (A) The customized PTFE sample holders (B) are filled with liquid agar so that biofilm can grow on the agar layer.
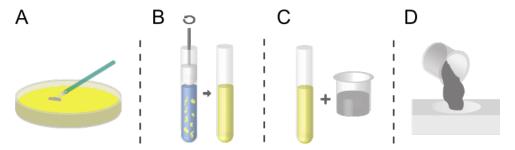


Figure 2.2: **Casting process of mortar samples:** (A) Fresh biofilm is harvested and pooled from agar plates and (B) an aqueous suspension is generated by grinding the biofilm with a pestle. (C) The suspension is mixed with cement and sand and (D) poured into the mortar casting form.

### 2.1.5 Mortar sample preparation

Fresh biofilm was prepared according to protocol *F1* and harvested from agar plates by manual scraping with a glass slide. The scraped biofilm material was pooled, weighed and split into small amounts as needed (Fig. 2.2A). For biofilm lyophilization, the scraped biofilm was pooled and freeze-dried for 24 h. Then, the lyophilized biofilm was stored at -80 °C until needed. Biofilm was mixed with 5 mL ddH$_2$O for a water/cement ratio of 0.5 (and with 6 and 7 mL, respectively, for wc values of 0.6/0.7). An aqueous suspension was generated by grinding the biofilm with a pestle for two minutes (Fig. 2.2B). This suspension was mixed with 30 g of CEN standard sand (DIN EN 196-1) and 10 g cement (CEM 42,5 N), stirred for two minutes (Fig. 2.2C), and poured into the casting form (Fig. 2.2D). The mortar samples were cured at room temperature for 3 days before used for any experiment.

## 2.2 Experimental techniques for biofilm characterization

To measure the material properties of different biofilm samples, a broad range of different experimental techniques were used to determine the viability, topology and viscoelastic properties of biofilms.

### 2.2.1 Minimal inhibitory concentration (MIC)

Different ionic solutions were prepared at increasing concentrations in LB medium. Each of those solutions was inoculated with 100 µL of an overnight culture of *B. subtilis* B-1 according to protocol *F1*. The chemically challenged cultures were incubated for 24 hours at 37 °C and the optical density was determined afterwards (Victor3 Multilabel Counter, PerkinElmer, Waltham, Massachusetts, USA).

### 2.2.2 Regrowth assay – planktonic bacteria

700 µL of an overnight culture of *B. subtilis* B-1 according to protocol *F1* was mixed with 700 µL of an ionic solution in micro test tubes. Tubes were placed onto a vertical lab rotator at 2 rpm for 1 hour to ensure good mixing. 10 µL of the chemically challenged culture were then transferred into 990 µL of fresh LB to remove the chemical challenge and allow for bacterial growth. Optical densities were determined (GeneQuant Pro, Amersham Biosciences, Amersham, UK) directly after mixing with fresh LB and after 15 hours of incubation at 37 °C and 90 rpm.

### 2.2.3 Regrowth assay – biofilm

For this assay, comparable amounts of untreated biofilm (~500 mg each) were weighed into sterile micro test tubes to ensure comparable starting conditions. 5 % (v/w) of a chemical stock solution was then added to the tubes and the chemical was distributed throughout the biofilm by gentle stirring with a pipette tip. After an incubation time of 1 hour, the micro test tubes containing the chemically treated biofilms were rinsed on the outside with ethanol to avoid contamination and placed into 50 mL centrifuge tubes, which then were filled with 20 mL of liquid LB medium. Those centrifuge tubes were mounted onto a lab shaker and incubated at 37 °C for 15 hours to wash out bacteria from the biofilm matrix and allow for their growth. Optical densities (GeneQuant Pro) of the bacterial solutions were then obtained every hour for a total duration of 15 hours.

### 2.2.4 Erosion assay

Customized sample holders were crafted from PTFE plates. Each sample holder has a cylindrical hole of 20 mm diameter and 3 mm depth. Sample holders were sterilized prior to filling with 1 mL of 1.5 % (w/v) agar containing LB generating a circular agar patch. Afterwards, 20 µL of an overnight culture was mixed with 80 µL of fresh LB and distributed over the agar surface of the sample holders. Sample holders were then incubated at 37 °C for 24 hours for biofilm growth. An example of such a biofilm-covered agar patch is depicted in Figure 2.3A. To conduct the erosion tests, 25 mL of a testing liquid was prepared and filled into centrifuge tubes. The sample holders were placed into the centrifuge tubes which in turn were mounted onto a lab shaker (Unimax 1010, Heidolph Instruments, Schwabach, Germany). The lab shaker was then set into rotation at 300 rpm for defined time intervals which generated a shear stress of about 1.6 mPa (Fig. 2.3B). After exposure to this shaking-induced shear force, the agar layer was carefully removed from the sample holder ensuring that the remaining
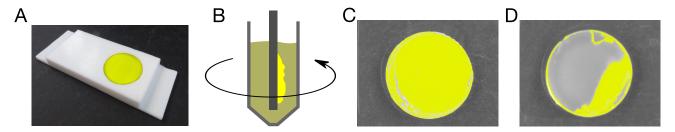
Figure 2.3: **Setup of the erosion experiment:** (A) A customized sample holder geometry containing a biofilm-covered agar patch is inserted into a tube which is then filled with a testing solution. (B) Shear forces are induced by setting the tube into rotational motion using a lab shaker. A biofilm-covered agar patch after an erosion experiment with a very low degree of erosion is depicted in (C). A high degree of erosion correlates with a lower coverage with biofilm after exposure to shear forces as depicted in (D). For clarity, the biofilm is colored in yellow in images A-D.

biofilm layer was not disturbed. Images of the biofilm-covered agar patches were acquired using a perimeter stand at a defined height with a digital camera (Canon PowerShot SX240 HS). Images were then converted into black and white using a binarization procedure implemented in the software ImageJ, and the percentage of biofilm erosion was calculated by determining the ratio of the area covered with biofilm and the total area of the agar patch (Fig. 2.3C+D).

The shear stress during the shaking procedure was calculated using the drag equation: $\frac{F_d}{A} = \frac{1}{2}\rho\nu^2 C_d$, where $F_d$ is the drag force in the direction of the flow velocity, $A$ is the reference area (31.41 mm²), $\rho$ is the density of the fluid (998 kg/m³), $\nu$ is the velocity of the object relative to the fluid (123.56 mm/s) and $C_d$ is the drag coefficient. The drag coefficient can be calculated using $C_d = \frac{0.455}{\log Re^{2.58}}$, where $Re$ is the Reynolds number for a horizontal flow along a plate. The Reynolds number is determined using $Re = \frac{w_\infty * x_u}{v}$, where $x_u$ is the length of the biofilm covered area (10.5 mm), $w_\infty$ the experimentally determined velocity (123.56 mm/s), and $v$ the kinematic viscosity of ddH$_2$O ($1\times10^6$ m²/s). The velocity was determined by recording a particle trajectory in the experimental setup.

### 2.2.5 Profilometry

A NanoFocus µsurf profilometer (NanoFocus AG, Oberhausen Germany) was used to obtain the surface profiles of one-day old biofilms. Three randomly selected spots with an area of 320x308 µm were scanned on each sample using a 50x objective. The biofilms were exposed for one hour to 2 mL of 99 % (or 80 %) ethanol as described in the biofilm treatment protocol *T2* above, and profilometer images were obtained before and after this treatment. The root-mean-squared roughness (*Sq*) was then determined by evaluating the scanned area with the software µsoft (Version 6.0, NanoFocus AG, Oberhausen, Germany) with the following formula: $Sq = \sqrt{\frac{1}{A}\iint\limits_{A} z^2(x,y)\,dx\,dy}$.
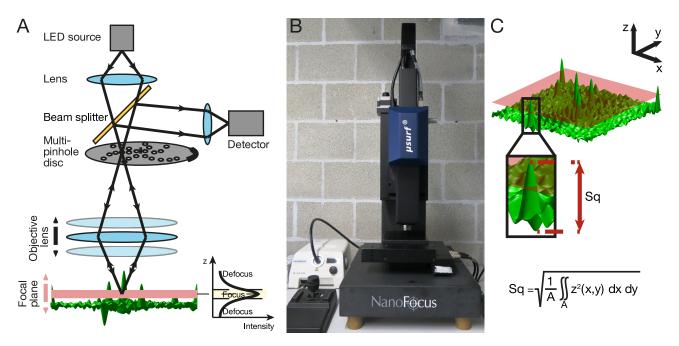
Figure 2.4: **Surface scanning with a profilometer:** (A) A laser diode is used to illuminate the sample. Only light reflected from the focal plane can pass through the observation pinhole and is measured with a detector. With consecutive scanning and changing the focal plane z-direction, the whole surface of the sample is scanned. (B) Image of the profilometer. (C) The root-mean-squared roughness parameter (*Sq*) is calculated from the acquired topological information of a sample

### 2.2.6 Macrorheology

Biofilms are commonly referred to as viscoelastic materials or complex fluids (39) and their mechanical properties are determined with a broad range of techniques. In this thesis, the shear modulus as determined by macrorheology was investigated and compared for biofilm samples.

The parameters describing the viscoelastic properties can be derived according to the two-plate model (Fig. 2.5A). The sample is located between two plates and will be sheared due to the movement of the upper plate. The lower plate is fixed in this setup. The force *F* and the area *A* define the shear stress $\tau = \frac{F}{A}$ on the sample. The resulting deformation $\gamma = \frac{\Delta x}{h}$ is defined as the movement of the upper plate $\Delta x$ with respect to the gap height *h*. With this information the shear modulus *G* can be calculated using the formula $G = \frac{\tau}{\gamma}$. However, this only describes the viscoelastic properties in a static state, and information on the time-dependence of the materials' response is still missing. To fully describe the viscoelastic behavior of a material, the shear stress is brought upon the sample in an oscillatory motion, *i.e.* a sinusoidal shear stress $\tau(t)$ is applied. The resulting deformation $\gamma(t)$ of this applied stress is recorded, and the phase shift $\theta$ (see Fig. 2.3C) is evaluated. For a purely elastic material this phase shift is $\theta = 0$, whereas the phase shift for a purely viscous material is $\theta = 90$. The complex shear modulus $G^{*}$(Equation 2.1) can now be used to calculate the two viscoelastic moduli, namely the storage modulus *G'* (Equation 2.2) and the loss modulus *G''* (Equation 2.3). The storage modulus represents the elastic response of the material, and the loss modulus the viscous response.
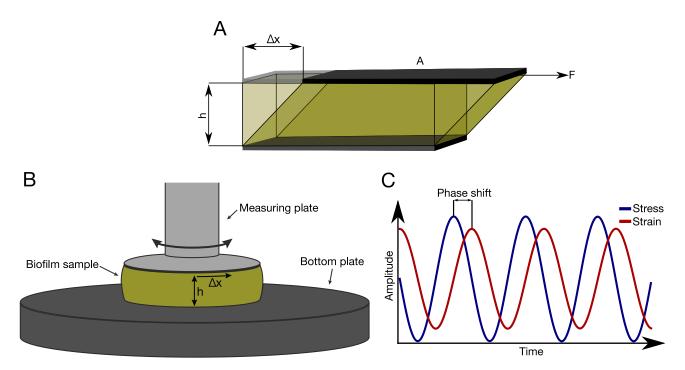
Figure 2.5: **Shear rheology with a macrorheometer:** (A) The two-plate model is used to derive the static shear modulus of a sample. (B) The sample is placed between the bottom plate and the measuring plate in a rheometer, and an oscillatory shear stress is applied to the sample. (C) The resulting strain and phase shift are used to determine the viscoelastic moduli.

$$G^* = \frac{\tau}{\gamma} \qquad (2.1)$$

$$G'(f) = \frac{T}{\gamma} \cos \theta \qquad (2.2)$$

$$G''(f) = \frac{T}{\gamma} \sin \theta \qquad (2.3)$$

The rheological measurements were performed using a commercial rheometer (MCR 302, Anton Paar GmbH, Graz, Austria). The rheometer can be driven in a stress- or a strain-controlled mode, however the strain-controlled mode has been proven to be more precise (40). Therefore, the following protocol was used to determine the viscoelastic moduli of bacterial biofilm samples:

- A sample was loaded into the rheometer and the gap was set to 300 µm.

- A torque of 0.5 µNm at a frequency of 1 Hz was applied to the sample. This low torque is set to ensure a response in the linear regime of the material. The resulting deformation $\gamma$ from this applied stress was recorded and multiplied with a factor of 1.5: $\gamma_{min}$ = $\gamma \times 1.5$.

- A frequency spectrum from 0.1 - 10 Hz was measured in strain-controlled mode with $\gamma_{min}$.

### 2.2.7 Elongational rheology

To measure the yield strength of bacterial biofilm, a custom-made elongational rheometer was built. A detailed description of the setup and the procedure can be found in Section 3.2.

### 2.2.8 Gene expression analysis

*B. subtilis* B-1 biofilms were grown and prepared as described in biofilm formation protocol *F2*. RNA for gene expression analysis was extracted from biofilms that were grown for 10 hrs and 18 hrs using the Quiagen RNeasy extraction kit following the protocols provided with the kit. Gene expression analysis was performed by IMGM Laboratories via quantitative real-time PCR (40 cycles) with custom TaqMan® Gene Expression Essays for the genes ywsC, blsA, epsH and tasA. As a positive control served the conserved 16S rRNA housekeeping gene. Negative controls did not contain genetic material or were performed with the corresponding RNA. This assay was performed by Sara Kesel.

### 2.2.9 AFM settings and cantilevers

Force spectroscopy was performed using a JPK NanoWizard® BioScience Atomic Force Microscope (with CellHesion® module, JPK Instruments AG). For measuring the elasticity of the biofilm surface, soft cantilevers with a silicon dioxide ($SiO_2$) bead with a diameter of 6.62 µm were used (sQube CP-PNPS-SiO-C-5, NanoAndMore GmbH). According to the manufacturers' data, the resonance frequency of the cantilevers were ~17 kHz and the cantilevers had a force constant of 0.08 N/m as verified using the thermal noise analysis (JPK Instruments Technical Note). For each individual cantilever the sensitivity (in nm/V) was calibrated by fitting the retract part of a force curve measured on plastic under ethanol, thus setting a baseline. Experiments were performed in contact mode using the following parameters of the control JPK software: sample rate 6000 Hz, z-length 20 µm, set-point 5.0 nN, speed 5.0 µm/s.

### 2.2.10 Surface indentation with AFM

After addition of ethanol, due to technical reasons, a minimum of ten minutes elapsed until the first measurement could be performed. Each biofilm surface was measured on three different positions. Each of these measurements was composed of 64 single runs measured with a distance of 1.25 µm to each other. For each strain 10 experiments were performed on 9 different days. The obtained force curves were analyzed with the JPK Data Processing Software (Version spm-5.1.7). To obtain the Young's Modulus, the Hertz model of elastic deformations was applied (41). A Poisson's ratio of 0.5 was set, assuming a perfectly incompressible material which deforms elastically. Although this introduces a certain error to the absolute values obtained, it does not interfere with relative statements. Further data analysis was performed using the software MATLAB (Version R2014a) and Igor Pro (Version 4.06). This assay was performed by Sara Kesel and Ina Gümperlein.

### 2.2.11 Determination of wet and dry mass of biofilm

To determine the wet mass of biofilms produced by the two *B. subtilis* wild-type strains NCIB 3610 and B-1, liquid cultures as described in biofilm formation protocol *F2* were confluently plated onto agar plates with 9 cm diameter and cultivated for 18 h. Part of the plates were covered with 99 % ethanol

for 1 h, in the presence or absence of γ-PGA. The ethanol was discarded and the plates were dried for 60 min. For all plates, treated and untreated, the biofilm was scraped from the agar and weighed in Eppendorf tubes. All tubes were frozen in liquid nitrogen at -169 °C and placed in an Alpha 1-2 lyophil (Christ, Osterode am Harz, Germany) at -55 °C and 0.021 mbar, where they were kept for 8 h. The tubes were weighed again to determine the dry mass. This assay was performed by Sara Kesel.

## 2.3 Experimental techniques for hybrid mortar characterization

### 2.3.1 Contact angle measurements

Three droplets of 20 μL ddH$_2$O were pipetted onto each mortar sample on different spots and images were acquired from a lateral view with a digital camera (Flea3, Point Grey, Richmond, Canada) using a varifocal lens with a focal length between 9 and 90 mm (Edmund Optics GmbH, Karlsruhe, Germany). The evaluation of the contact angle was performed using the image analysis software ImageJ with a drop analysis plugin tool (42).

### 2.3.2 Profilometry

A NanoFocus μsurf profilometer (NanoFocus AG, Oberhausen Germany) was used to obtain the surface profiles of hybrid mortar samples. Three randomly selected spots with an area of 320x308 μm were scanned on each sample using a 50x objective. The *Sq* value was then determined as described above.

### 2.3.3 Water uptake experiments

X-ray dark-field imaging was performed together with Marwa Tallawi and Fritz Prade from the physics department of the TUM. The laboratory setup was equipped with a commercial microfocus tube which was operated at 60 kV and a power of 100 W. A standard flat-panel detector with a pixel-size of 127 μm and a CsI scintillator was used for image acquisition. The interferometer consisted of a source-, a phase- and an analyzer-grating which were symmetrically aligned along the beam axis. The distance between the source- and phase-grating as well as the distance between the phase- and the analyzer-grating was 92.5 cm. The grating periods were 10 μm for the source- and analyzer-grating and 5 μm for the phase-grating. The grating bars of G0 and G2 were made of gold with a height of 160–170 μm while nickel with a height of 8 μm was used for the grating G1. This height corresponds to a phase-shift of π/2 at a X-ray design energy of 45 keV. The distance of G2 to G1 corresponded to the first fractional Talbot-distance. The experiment was conducted on two samples of standard mortar and two samples of modified hybrid mortar and repeated trice. The mortar samples for X-ray imaging were cast into a four-chamber PTFE sample holder. After curing but prior to the water uptake experiment, the samples were covered with a polyimide film tape to prevent water evaporation from the samples during the experiment. The bottom of the samples remained uncovered so that the samples could be

exposed to water. A plastic container filled with $ddH_2O$ was introduced at the bottom of the field of view. Twenty X-ray radiographs were acquired before the samples were submerged into the water. The sample holder was moved down to submerge the bottom parts of the samples into water for about 2 mm. Directly after immersion, X-ray radiographs were acquired continuously to determine the capillary water uptake. The overall experiment lasted approximately 24 h. During the first hour, the images were taken continuously every 10 s with an exposure time of 8 s per projection, whereas in the following 23 h images were taken every 300 s (43).

### 2.3.4 Scanning electron microscopy (SEM)

A scanning electron microscope (JEOL-JSM-6060LV, Jeol, Eching, Germany) was used to study the nanoscopic surface morphology of the hybrid mortar samples. For cross-sectional images, the mortar samples were separated vertically into two halves with a saw. Afterwards, all specimens were glued to aluminum stubs and sputtered with gold (MED 020, BAL-TEC, Balzers, Liechtenstein). Images were acquired at an acceleration voltage of 20 kV and a spot size of 30 nm. The images were acquired by Kathrin Boettcher.

### 2.3.5 X-Ray photoelectron spectroscopy (XPS)

XPS analysis was performed using a LHS-10 spectrometer (Leybold Heraeus GmbH, Hanau, Germany) equipped with a monochromated AlK$\alpha$ (h$\nu$ = 1486.6 eV) X-ray source operating at 12 kV and 10 mA. The samples were prepared by scratching the mortar surface to obtain powder. Then, the powder was pressed smoothly onto conducting double adhesive copper foil using a spatula, and the foil was fixed onto an aluminum sample holder with three cavities. The area for the XPS analysis was 3 mm in diameter, and high vacuum ($4.7x10^{-8}$ m bar) was applied for measurements. Depending on the signal-to-noise ratio of the measurements, 5–20 scans were averaged per sample. XPS analysis was performed by Marwa Tallawi.

# Material properties of bacterial biofilms

## 3.1 Mechanical and chemical resilience of biofilms

Biofilms can form in adverse and challenging environments such as pipes in industrial settings or on surfaces in food production. Therefore, quantifying and understanding the material properties of bacterial biofilms has become a main goal of biofilm research. This knowledge is not only important for the deactivation of biofilms but also for the development of removal strategies. For instance, to remove biofilms in pipes, it is important to know which forces a biofilm can withstand before the biofilm is flushed away, but also how different chemicals change this behavior. However, data on these biofilm properties is rare since a quantification of such parameters is complicated: flushing large amounts of chemicals through pipes is rather impractical, and even in such a scenario, the determination of the amount of removed biofilm is difficult. Conversely, dedicated measuring setups to determine biofilm removal efficiency are rare (44–48). Usually, biofilm growth times are in the range of several days to weeks, and chemical influences on the biofilm properties can hardly be integrated into the mentioned setups.

Therefore, a new erosion assay, similar to the macroscopic erosion test introduced by Simões *et. al*(47), was developed in this thesis, however, in a miniaturized version to render it more high-throughput compatible (see Sec. 2.2.4 for details). In short, biofilm is grown on customized PTFE sample holders and shear forces are induced by shaking the sample in a liquid solution, mimicking water flow. The percentage of biofilm removal over time is then determined optically. The following chapter was mainly adopted from the publication Grumbein *et. al*(10).

### 3.1.1 Erosion of bacterial biofilms

As a first test, the removal efficiency of biofilm is determined when shear forces are induced by agitating the biofilm samples in $ddH_2O$. The first measurable erosion can be detected after about 5 minutes, and following this initial erosion, a linear increase in biofilm removal with time can be observed. After 25 minutes, half of the biofilm is removed, and more than 90 % of the biofilm is washed off the surface after ~40 minutes (Fig. 3.1A). To demonstrate that the optical analysis correctly measures the degree of biofilm removal as a function of time, the eroded biofilm mass is determined by a second, independent method: here the liquid in which the erosion assay was performed was freeze-dried and the eroded biomass was determined by weighing the lyophilized material. A similar linear increase can
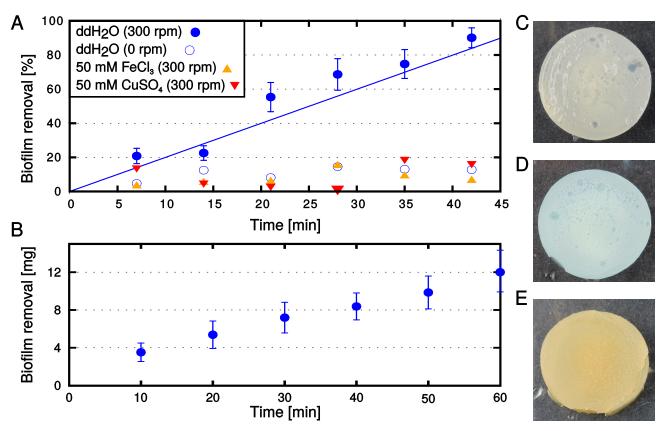
Figure 3.1: **Erosion of biofilm:** (A) *B. subtilis* B-1 removal in ddH$_2$O is negligible in the absence of shear forces (empty circles, blue). However when this erosion experiment is repeated in the presence of a shear force, the removal of biofilm increases linearly with time (full circles, blue). In contrast, when the erosion test is performed in 50 mM FeCl$_3$ (triangles, red) or 50 mM CuSO$_4$ (inverted triangles, orange), the degree of biofilm erosion is greatly reduced. (B) *B. subtilis* B-1 removal in ddH$_2$O as determined by lyophilization of eroded biofilm mass in the liquid. The color of an untreated biofilm (C) is significantly altered after incubation with 50 mM CuSO$_4$ (D) or 50 mM FeCl$_3$ (E) for 1 hour.

be observed with this second method (Fig. 3.1B) which verifies the suitability of the erosion assay to quantify the stability of *B. subtilis* B-1 biofilms towards shear forces.

The results of these first experiments indicate that a prolonged application of shear forces in an aqueous environment can lead to a removal of biofilm mass. However, swelling of the biofilm in water could also contribute to the observed erosion process. Therefore, the experiment was repeated, but this time, the samples were placed in ddH$_2$O, and no shear forces were induced. In the absence of shear forces, the degree of biofilm erosion is much lower and saturates at ~10 % after 15 minutes (Fig. 3.1A). This clearly demonstrates that *B. subtilis* B-1 biofilms are sensitive towards shear forces as they may occur in liquid environments such as river beds or waste water pipes. However, in their natural environment, biofilms are able to withstand shear forces, *e.g.* when they grow on the surface of pipes or catheters in the presence of flowing fluids. This clearly indicates the existence of a mechanism that allows biofilms to grow in such environments and protect themselves from erosion. One explanation could be that in pipes or catheters the biofilms are exposed to a more complex chemical environment

than ddH$_2$O. Thus, the question arises whether and how variations in the chemical composition of the aqueous environment affect the erosion stability of *B. subtilis* B-1 biofilms.

One difference in the chemical environment biofilms are exposed to in pipes is the material these pipes are made of. Examples of common pipe materials are copper and iron, which in turn release Cu$^{2+}$ and Fe$^{3+}$ ions into the water stream (49). Thus, the next step is to test whether the presence of Cu$^{2+}$ and Fe$^{3+}$ ions influences the erosion stability of *B. subtilis* B-1 biofilms, and the erosion assay was repeated with biofilm samples treated with those ions. More precisely, the biofilm samples were exposed to solutions of 50 mM CuSO$_4$ and 50 mM FeCl$_3$ instead of ddH$_2$O. In the presence of Cu$^{2+}$ ions, the measured biofilm erosion is comparable to when the biofilm was placed in ddH$_2$O without applying shear forces: over a time span of 42 minutes, less than 20 % of the biofilm was removed. When a 50 mM FeCl$_3$ solution was used, the same stabilization effect was obtained. In addition to this stabilization effect, a change in the material quality of the biofilm can be observed. For both ions, the color of the biofilm is altered after incubation: whereas the biofilm acquires an orange/brown color after exposure to FeCl$_3$ (Fig. 3.1E), it turns blue after exposure to CuSO$_4$ (Fig. 3.1D). This clearly indicates an uptake of the respective ions into the biofilm matrix. Moreover, a significant stiffening of the biofilm matrix could be observed, when trying to remove these biofilms from the agar surface by manual scraping. This indicates that the incorporation of Cu$^{2+}$ and Fe$^{3+}$ ions into the biofilm material might induce a change in stiffness of the biofilm matrix.

### 3.1.2  Viscoelastic properties of bacterial biofilms

To quantify the putative alterations in biofilm stiffness observed from manual scraping, the viscoelastic properties of *B. subtilis* B-1 biofilms which have been exposed to selected chemicals were measured. As a material parameter describing the viscoelastic properties of the biofilm in response to shear forces, the dynamic shear modulus $G^*$, or more precisely the storage modulus $G'$ and loss modulus $G''$ were chosen. Experimentally, those viscoelastic moduli are determined from the in-phase and out-of-phase part of the biofilm deformation in response to an oscillatory shear force (Fig. 2.5C). The viscoelastic moduli are measured over a range of biologically relevant frequencies, *i.e.* between 100 mHz and 10 Hz corresponding to time scales of 0.1 to 10 s. For untreated biofilm, the storage modulus dominates over the loss modulus over the whole frequency regime tested for pure biofilm (Fig. 3.2) underscoring the pronounced elastic properties of a bacterial biofilm in contrast to the purely viscous properties of a bacterial suspension. Furthermore, *B. subtilis* biofilms obtained from different growth batches show relatively little variation in their viscoelastic properties, and the measured $G'$ values are in the range of 50 to 125 Pa.

Yet, it is unclear if the scraping process and transfer of the samples significantly alter the complex microarchitecture of the biofilm. To test this, *B. subtilis* B-1 was grown in the rheometer *in situ* with a special adapter. This adapter, a so called submersion flow cell, consists of a lower plate, which is connected via small holes with a reservoir beneath, which allows the biofilm to grow at the plate interface and at the same time, the biofilm is provided with nutrition from the liquid media in the reservoir
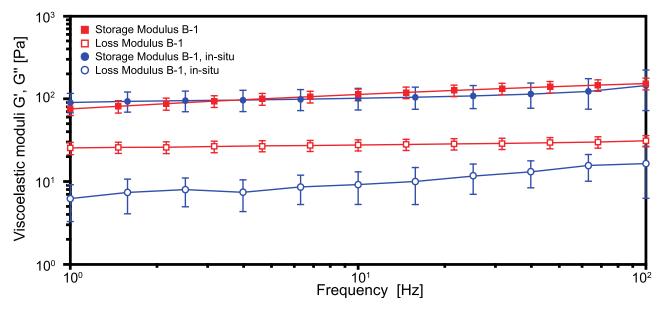
Figure 3.2: **Viscoelastic properties of *B. subtilis* B-1 biofilms:** The viscoelastic response of *in situ* grown biofilms (squares, blue) is only minimally changed compared to when biofilms are scraped from agar, pooled and transferred to the rheometer (circles, red).

beneath. Biofilms were grown overnight at a temperature of 37 °C and the viscoelastic properties were determined afterwards. No significant differences were detected in the elastic modulus of *in situ* grown compared to normally grown biofilm samples (Fig. 3.2). Furthermore, the use of this growth method is impractical as only a single sample can be measured per day and the risk of a contamination with air-born bacteria is drastically increased. Therefore, biofilms grown according to biofilm formation protocol *F2* were used for the rheological characterization.

Yet, it is not clear whether the effect a given chemical might have on the viscoelastic properties of the biofilm is immediate or needs a certain time span until the maximum effect is reached. Therefore, *B. subtilis* B-1 biofilms were covered with a 50 mM $FeCl_3$ or 50 mM $CuSO_4$ solution for short time intervals as described in treatment protocol *T2* (see Sec. 2.1.3) prior to harvesting of the samples. A fast increase of both viscoelastic moduli could be observed within the first 10-15 minutes (Fig. 3.3A+B). The increase in biofilm elasticity saturated after approximately 20 minutes for both ions and the final storage moduli lay in the range of several hundred kPa. Thus, 60 minutes is chosen as a suitable exposure time of biofilms to chemicals and to determine the effect of such a chemical on the viscoelastic properties. This ensures that the maximum effect a given chemical might have on the viscoelastic properties of the biofilm is reached. However, treatment protocol *T2* is not well suited to test the effect of a broad range of chemicals since large amounts of a solution is needed, the handling of the covered plates is challenging, and the amount of ions taken up by the biofilm is unknown. Therefore an adjusted treatment protocol *T1* was established: by adding only small amounts (5 %(v/w)) of a high-concentrated stock solution to the harvested biofilm samples it is ensured that the final concentration of chemicals in biofilm samples is known and identical for all samples.
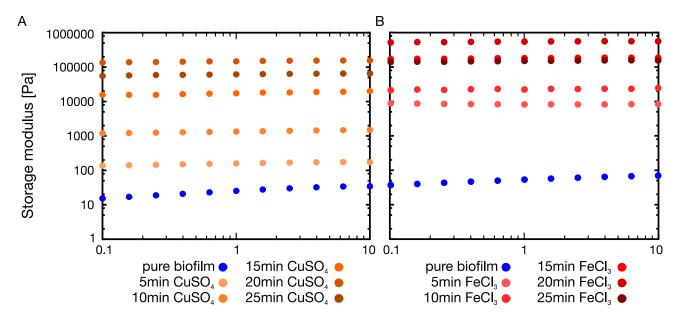
Figure 3.3: **Time dependence of biofilm elasticity after exposure to metal ions:** *B. subtilis* B-1 biofilms are treated with 50 mM CuSO$_4$ (A) and 50 mM FeCl$_3$ (B) for short time intervals. The elasticity is increasing over the first 10-15 minutes and saturates after approximately 20 minutes. For clarity, only the storage modulus is depicted in the graph.

The rheological characterization was repeated with the new protocol *T1*, and as a negative control ddH$_2$O was added to the biofilm. The effect on the viscoelastic properties, namely the storage and the loss modulus, by this slight dilution of the biofilm material was only minimal (Fig. 3.4). As a next step, 5 %(v/w) of a 1 M stock solution of FeCl$_3$ and CuSO$_4$ was added to the biofilm, resulting in a final concentration of 50 mM FeCl$_3$ and 50 mM CuSO$_4$. Here, differences in the amount of stiffening of the biofilm matrix can be observed in the viscoelastic moduli: both viscoelastic moduli increase by two orders of magnitude when CuSO$_4$ is added, whereas the effect is even more pronounced for the addition of FeCl$_3$ (Fig. 3.4). However, the dependence of the viscoelastic moduli on the shear frequency remains weak. Thus, the viscoelastic behavior of the biofilms can be subsumed into a single material parameter. For simplicity, the plateau modulus $G_0 = G'(1 \text{ Hz})$ was chosen to compare the elastic properties of bacterial biofilms.

Both FeCl$_3$ and CuSO$_4$ form acidic solutions in water, and it is not clear whether the observed alterations arise from the metal ions or are caused by pH differences. Therefore, the rheological experiment was repeated with aqueous solutions buffered to pH 3, 7 and 10. Since the viscoelastic moduli remain unaffected by those pH alterations, the change in biofilm stiffness observed for CuSO$_4$ and FeCl$_3$ is indeed caused by the ions (Fig. 3.5A, upper panel). Now, the question arises whether such a stiffening of the biofilm matrix can be achieved by Cu$^{2+}$ and Fe$^{3+}$ ions only, or if other ions show similar effects. For this purpose, a rheological screening was performed with biofilms treated with other metal ions ranging from monovalent ions such as Na$^+$ or K$^+$ to multivalent ions such as Mg$^{2+}$ or Al$^{3+}$. As the naturally grown biofilm might already contain a significant amount of ions, chelating agents such as citrate, EDTA and EGTA also were tested. To maximize putative effects of the used
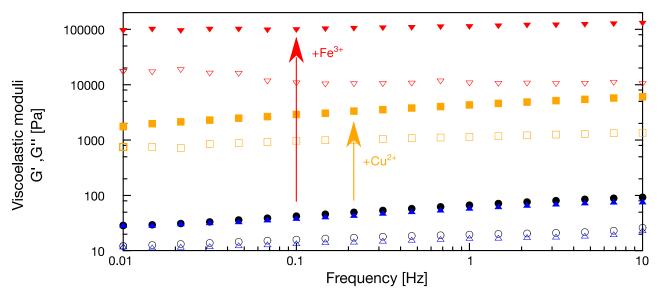
Figure 3.4: **Viscoelastic properties of *B. subtilis* B-1 biofilms:** The viscoelastic response of pure biofilms (triangles, blue) is only minimally changed by the addition of $ddH_2O$ (circles, black). After treatment with 50 mM $CuSO_4$ (squares, orange) and 50 mM $FeCl_3$ (inverted triangles, red), both moduli show a significant increase. The storage modulus $G'$ is depicted by closed symbols and the loss modulus $G''$ is depicted by the corresponding open symbols.

chemicals, stock solutions close to the solubility of the respective chemical were used when adding 5 % (v/w) of a chemical to the biofilm matrix for rheological evaluation.

For most chemicals tested, a change of biofilm elasticity cannot be detected. Neither chelating agents nor monovalent ions induce a change in the elastic properties of the biofilm. In contrast, some multivalent ions ($Cu^{2+}$, $Zn^{2+}$, $Fe^{3+}$, $Al^{3+}$) induce a significant fortification of the biofilm material, whereas others, *i.e.* $Fe^{2+}$ only weakly change the elastic properties or as *e.g.* $Mg^{2+}$ and $Ca^{2+}$, hardly alter the biofilm stiffness at all (Fig. 3.5A, upper panel).

### 3.1.3 Influence of chemicals on biofilm properties

So far, it was shown that $Cu^{2+}$ and $Fe^{3+}$ ions protect *B. subtilis* B-1 biofilms from erosion and, at the same time induce a stiffening of the biofilm matrix. The erosion assay was therefore expanded to the other ions and chemicals used for the rheological characterization. The idea is to test whether a change in the bulk material properties might be responsible for the erosion protection of *B. subtilis* B-1 biofilms. To ensure comparable results, the concentrations of the erosion assay were matched to the final concentrations used in the macrorheological screening. In addition to $Cu^{2+}$ and $Fe^{3+}$, also the multivalent ions $Ca^{2+}$, $Zn^{2+}$, $Fe^{2+}$, and $Al^{3+}$ reduced biofilm erosion. Monovalent ions and chelating agents neither induce a stiffening of the biofilm matrix nor protect biofilms from erosion (Fig. 3.5A, lower panel). This leads to the notion that erosion protection and stiffening of the biofilm matrix are two related phenomena. However, in the case of $CaCl_2$, erosion protection was achieved without a measurable stiffening of the biofilm matrix. This indicates that other biofilm properties besides their
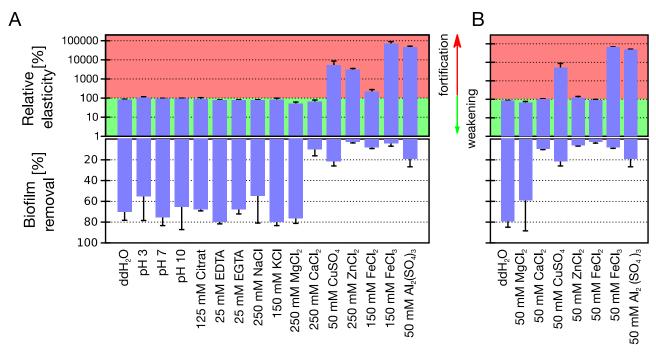
Figure 3.5: **Comparison of viscoelastic properties and erosion efficiency:** (A) Maximal influence of different chemical conditions and (B) direct comparison of identical concentrations of multivalent metal ions on the shear elasticity and erosion stability of *B. subtilis* B-1 biofilms. The elasticity of the biofilm (upper panel) has been normalized by the elastic modulus obtained for an untreated biofilm sample. Values in the red area depict a mechanical fortification of the biofilm whereas values in the green area depict a weakening of the biofilm, compared to an untreated sample. The erosion efficiency (lower panel) was quantified by determining the percentage of biofilm removal in solutions of the corresponding chemical.

shear stiffness might play a role in their stability towards shear forces in fluid flow.

To further test this hypothesis, the screening was repeated with lower concentrations, to find out whether the increase in shear stiffness depends on the ion concentration. If, at those lower concentrations, a biofilm still is protected from erosion without showing an increased shear stiffness, it would underscore the hypothesis that those biofilm properties are not necessarily linked. Both the macrorheological and the erosion assay were repeated with multivalent ions only, since all other chemicals showed no effect at the concentrations used before. At this lower concentration, *i.e.* 50 mM for all ions, only $Cu^{2+}$, $Fe^{3+}$, and $Al^{3+}$ showed an increase in biofilm elasticity. However, additionally to those three ions, biofilms treated with $Ca^{2+}$, $Zn^{2+}$, and $Fe^{2+}$ were also protected from erosion, although they showed no significant alteration in biofilm elasticity (Fig. 3.5B). Apparently, there are several conditions where erosion protection was achieved without a significant increase in biofilm shear stiffness. This shows that those two biofilm properties are not necessarily linked and should be treated as independent biofilm properties.
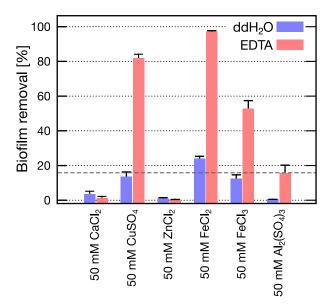
Figure 3.6: **Persistence of erosion stability:** *B. subtilis* B-1 erosion stability in ddH$_2$O (blue) and 25 mM EDTA (red) after pre-treatment in 50 mM solutions of metal ions.

### 3.1.4   Persistence of erosion stability

The results presented so far show that most multivalent ions can stabilize the biofilm matrix and/or protect the biofilm against shear forces induced by a liquid flow. However, in industrial or biological settings the chemical environment might significantly change over time. This raises the question whether this effect can persist, once the stabilizing ions are not present in the surrounding liquid anymore. To test this, the erosion assay was repeated with a change in chemical condition: the biofilm samples were pre-treated by incubating them for ~40 minutes in a solution containing 50 mM of a metal ion solution. After this incubation time, the samples were transferred into ddH$_2$O and the erosion assay was performed as in the previous erosion experiment. The stabilizing effect induced by the metal ions persisted, which indicates that the metal ions were absorbed and strongly bound by the biofilm matrix (Fig. 3.6). However, a strong chelating agent might be able to remove those ions from the biofilm matrix. To test this hypothesis a solution containing the chelating agent EDTA was used instead of ddH$_2$O after the treatment with metal ions. Since EDTA is known to form highly stable chelate complexes with metal ions, a 25 mM solution of this chelating agent might be sufficient to remove the ions from biofilm matrix. Indeed, EDTA was able to render biofilms sensitive to erosion again, even if they had been treated with Cu$^{2+}$, Fe$^{2+}$, or Fe$^{3+}$ ions. Also the change of color due to the incorporation of ions into the matrix was reverted back to that of untreated biofilms. In contrast, for biofilms treated with CaCl$_2$, ZnCl$_2$, and Al$_2$(SO$_4$)$_3$, the stabilizing effect remained when the erosion assay was performed in an EDTA solution (Fig. 3.6).
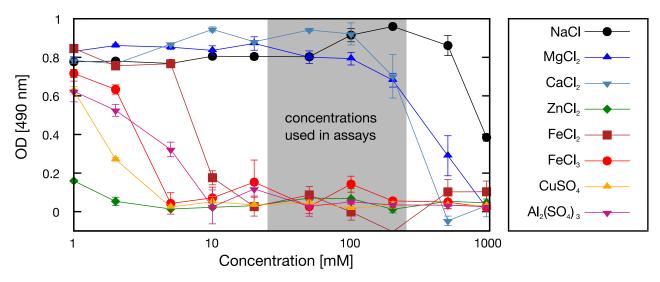
Figure 3.7: **Minimal Inhibitory Concentration:** Growth of planktonic *B. subtilis* B-1 in increasing concentrations of metal ions used for rheological characterization and erosion assay.

### 3.1.5 Toxicity of metal ions

So far, the effect of different chemicals on the mechanical characteristics of biofilm was investigated. It was shown that metal ions which were incorporated into the biofilm matrix, can induce a stiffening of the matrix and/or protect the biofilm from erosion due to shear forces. The chelating agent EDTA was able to remove selected metal ions from the biofilm matrix, reverting the previous effects. However, the effect of the metal ions on the biofilm embedded bacteria is unclear. Even though the bacterial metabolism depends on certain metal ions, *e.g.* $Fe^{3+}$(50), these ions may become toxic for bacteria at increased concentrations. To test this, a minimal inhibitory concentration (MIC) assay was performed with the metal ions used for the macrorheological screening and the erosion assay. The obtained results show that in terms of toxicity, the tested ions can be subdivided into two groups. The first group (NaCl, $MgCl_2$, and $CaCl_2$), inhibited the growth only at high concentrations, *i.e.* at concentrations higher as the concentrations used in the assays presented before. The second group of metal ions ($CuSO_4$, $FeCl_2$, $FeCl_3$, $Al_2(SO_4)_3$, and $ZnCl_2$), already inhibited bacterial growth at concentrations of 10 mM or even lower (Fig. 3.7).

The MIC describes the concentration at which a given chemical inhibits the growth of bacteria. However, there are in principle two ways how chemicals might harm bacteria. First, the chemical might inhibit bacterial growth, but once after the chemical pressure is released, bacterial growth will continue (bacteriostatic). A second possibility is that the concentration may be toxic and induce bacterial death (bactericide). To test the latter, a regrowth assay was performed and planktonic *B. subtilis* B-1 bacteria were challenged with high concentrations of metal ions. Afterwards, the bacteria were transferred to fresh LB to remove the chemical pressure. The optical density was then measured to test whether the bacteria survived. As depicted in Table 3.1, the results mostly matched the MIC assay. However, in the case of $FeCl_2$, a concentration of 150 mM was sufficient to inhibit bacterial growth, but the bacteria

| *B. subtilis* B-1 | ddH$_2$O | 250 mM NaCl | 250 mM CaCl$_2$ | 250 mM MgCl$_2$ | 150 mM FeCl$_2$ | 150 mM FeCl$_3$ | 50 mM CuSO$_4$ | 50 mM Al$_2$(SO$_4$)$_3$ | 250 mM ZnCl$_2$ |
|---|---|---|---|---|---|---|---|---|---|
| Planktonic | + | + | + | + | + | - | - | - | - |
| Biofilm embedded | + | + | + | + | + | + | + | + | - |

Table 3.1: **Viability of planktonic and biofilm embedded *B. subtilis* B-1.** Growth after chemical challenge is indicated by +, and a lack of growth is indicated by -.
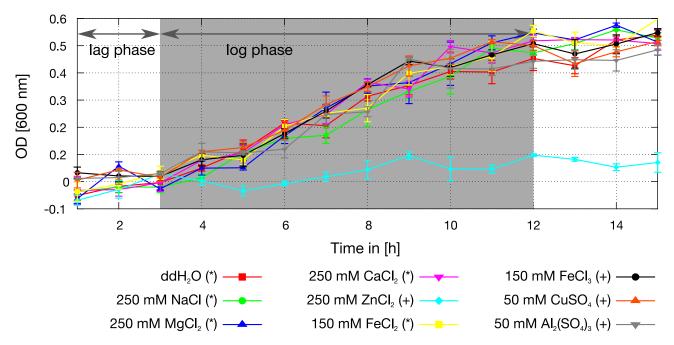


Figure 3.8: **Bacterial growth after chemical treatment of biofilms:** Growth of *B. subtilis* B-1 biofilm embedded cells after treatment with solutions of metal ions. * indicates growth of planktonic *B. subtilis* B-1 cells after treatment, whereas + indicates no growth.

were able to grow again once the chemical pressure was released. The experiment revealed that FeCl$_2$, NaCl, MgCl$_2$, and CaCl$_2$ are bacteriostatic, whereas 150 mM FeCl$_3$, 50 mM CuSO$_4$, 50 mM Al$_2$(SO$_4$)$_3$ and 250 mM ZnCl$_2$ are bactericide. One drawback of this test was that only the toxicity towards planktonic bacteria was determined, and the biofilm matrix was not taken into account. For antibiotics, it was already shown that the biofilm matrix protects embedded cells and the diffusion of antibiotics is retarded in the biofilm matrix (51, 52), which might also be true for other substances or chemicals. Therefore, the assay was repeated with the same chemical concentrations of metal ions, but this time with chemically challenged biofilms instead of planktonic bacteria. The results show that only a 250 mM ZnCl$_2$ solution was lethal for biofilm embedded bacteria. For all other metal ions tested, biofilm embedded bacteria were able to grow again once the chemical pressure was released (Table 3.1 and Fig. 3.8).

The results demonstrate that certain chemicals can permanently suppress bacterial growth in biofilms, even after the chemical pressure is released again. However, most chemicals seem to be trapped by the biofilm matrix in such a way that they are not able to harm embedded bacteria.

### 3.1.6 Discussion

In this chapter, a new biofilm assay to determine the erosion resistance of *B. subtilis* B-1 biofilms in fluid flow was presented. With this assay, it is possible to detect the time-dependent erosion process in varying chemical environments. The influences of those chemical environments on biofilms was also investigated with a macrorheological assay. As a model system for bacterial biofilms, biofilms formed by the strain *B. subtilis* B-1 were investigated. With a sufficient supply of nutrition, this strain is able to produce large amounts of biomass in a short time, *i.e.* ~1500 mg can be harvested from standard petri-dishes after incubation for only 24 h. This fast growth and large production of biomass renders this biofilm variant very convenient for the macrorheological characterization and erosion assay used here. In principle, all other biofilm variants that grow reasonably well on agar can be used in the assays presented here.

The developed setup is advantageous over other methods that have been introduced to study biofilm erosion: for instance, the assay by Simões *et. al*(47) is able to determine the decrease in biomass of biofilms on a macroscopic scale. Biofilms are grown on metal cylinders with a surface of 34.6 cm$^2$ and afterwards rotated in a chemical bath. However, to ensure full coverage of the metal cylinders, the biofilm needs to be grown for several days and the experiment is therefore very time-consuming. Thus, it is not convenient to screen a broad range of chemical conditions. Other methods make use of microfluidic approaches (53) and determine the dynamic detachment process of biofilms. However, a quantitative comparison of the influence of different chemicals on the erosion process is difficult to obtain. In contrast, the assay developed here is able to quantify the erosion process and miniaturizes the area of biofilm growth to 3.1 cm$^2$. The use of an optical method to detect the biofilm erosion renders the assay a cost-efficient and easy-to-handle platform for high-throughput screening of chemicals that are considered for biofilm removal.

It was shown that the absorption of metal ions does not only protect *B. subtilis* B-1 biofilms from erosion, but also induces a stiffening of the biofilm matrix. Even though the concentrations tested here are beyond typical release values of metal ions in water distribution systems (54), an accumulation of those ions in the biofilm matrix could still occur. An indication for such an accumulation was found in the macrorheological assay when the different biofilm treatment protocols *T1* and *T2* were used. When covered with a solution of 50 mM CuSO$_4$ (*T2*), an increase of 3–4 orders of magnitude was observed. However, when a 50 mM CuSO$_4$ solution was forced into the biofilm (*T1*), this increase was only two orders of magnitude. This suggests that the concentration of Cu$^{2+}$ ions incorporated into the biofilm matrix is higher than in the surrounding liquid. However, this is only possible if the Cu$^{2+}$ ions have a high affinity for the biofilm matrix components, a notion which agrees well with the result that the strong chelating agent EDTA cannot easily wash out all absorbed metal ions (Fig. 3.6).

The absorbed metal ions could be responsible for an increased matrix stiffness, since those metal ions could ionically cross-link the biofilm matrix (3). This hypothesis is supported by the fact that the polyanionic biopolymer γ-PGA is a main component of the biofilm matrix formed by *B. subtilis* B-1 (13). Therefore, cross-linking should be possible *per se*, but on the other hand, it has been shown that also other biofilm matrices containing polyanionic biopolymers, *e.g.* alginate, exhibit a fortification

of the biofilm matrix upon treatment with metal ions (9, 55). However, for those biofilms, ionic cross-linking was not sufficient to account for the observed increase in biofilm stiffness since only trivalent ions had a significant effect.  An even higher degree of specificity was found for the biofilm matrix of *B. subtilis* B-1, since only selected metal ions caused an effect.  This high degree of specificity is also reflected when the different metal ions are compared with respect to their enhancement on the erosion stability and their ability to induce a matrix fortification. Furthermore, the ability of metal ions to harm bacteria also depends highly on the used metal ion. Even though high concentrations of metal ions were used, only $ZnCl_2$ was able to kill the embedded bacterial population.  However, the two determined biofilm parameters, *i.e.* the erosion stability and viscoelastic properties, are not linked to the viability of the cells, and indeed can be altered without harming the embedded bacteria. This seems to be a common feature among biofilms since other studies have reported similar findings (9, 56, 57). Biofilm embedded bacteria are more resistant towards heavy metals than planktonic cells (58), and bind metals in different quantities (59). This ability of *B. subtilis* B-1 biofilms to deactivate toxic ions by absorption into the biofilm matrix and - on top of that - even utilize them to improve the mechanical performance of the biofilm can be regarded as a well-tailored strategy to survive in potentially harmful environments (60).

## 3.2   Elongational rheology of biofilms

In the previous chapter, the erosion stability of *B. subtilis* B-1 biofilms in response to fluid shear and the change of the viscoelastic properties upon treatment with metal ions were determined. In both cases, the forces exerted onto the biofilms were shear forces. However, in natural settings, the occurring forces are not limited to shear forces only, but instead tensile forces, or a combination of both forces act simultaneously on a biofilm. Therefore, the approach in the previous chapter to determine material properties of bacterial biofilms has to be developed further, and elongational forces need to be considered as well when the material properties of biofilms are determined. For artificial materials, the properties in response to tensile forces can be determined relatively simply, since a great variety of testing stands is available. Conversely, this available testing equipment usually is not applicable to biological samples, as the forces occurring in biological systems are often very low, and the mounting of biological samples to these test stands is in many cases difficult. Therefore, suitable characterization methods for soft biological materials such as bacterial biofilms are rare, and, when it comes to *in situ* testing, they are almost non existent.

### 3.2.1   Experimental setup

To measure elongational rheology of bacterial biofilm samples *in situ*, a dedicated measurement setup was developed. The following section will describe the requirements for such a test stand and the parts and methods that are needed to fulfill this task.

**General layout**

To ensure that biofilms can be measured in their natural grown state special care had to be taken during the construction process. Usually, samples for tensile testing are prepared in such a way that they can be fixed directly into the setups. However, such an approach is not applicable to biofilm samples, since bacteria need to be grown on some sort of nutrition layer to form a biofilm. Harvesting and transferring those samples into a testing setup could, however, damage the complex microarchitecture of those biofilms. This may alter the material properties of the biofilm such that the measured results do not reflect the 'true' biofilm properties. A second requirement for the testing equipment is that it should be possible to treat the biofilm samples with chemicals while fixed in the experimental setup. Results from the macrorheological screening assay discussed in Section 3.1.3 revealed, exposure to *e.g.* metal ions can drastically change the mechanical properties of biofilms. The results obtained there showed that the influence of the chemicals on the biofilms properties is observed directly after the treatment. Therefore, the time between sample treatment and the measurement procedure needs to be kept short. To achieve this, the whole setup was constructed horizontally to allow for such a biofilm treatment directly in the measuring setup. In such a horizontal alignment however, the sample holders cannot be mounted directly to the force sensor, but instead some kind of support needs to be used to decouple the force sensor and the sample holders. This support needs to carry the sample

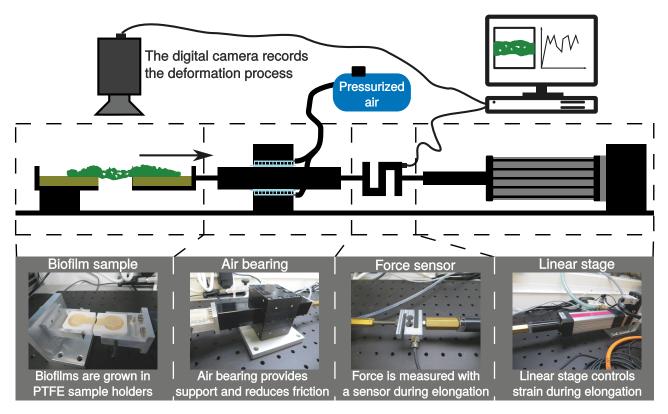| Biofilm sample | Air bearing | Force sensor | Linear stage |
|---|---|---|---|
| Biofilms are grown in PTFE sample holders | Air bearing provides support and reduces friction | Force is measured with a sensor during elongation | Linear stage controls strain during elongation |

Figure 3.9: **Layout of the measuring setup.** A schematic of the stretching device with the key elements of the device: (A) the sample holder for biofilm samples grown *in situ*, (B) the air-bearing as support, (C) the force sensor, (D) and the linear stage for the movement of the sample. The rupture process is followed with a camera and the force data is recorded with a computer.

weight on the one hand, and transmit the forces arising from the stretching experiments on the other hand. A bearing is introduced to connect the force sensor with the sample holder part. This prevents measurement errors due to lateral forces and also protects the fragile force sensor from breaking. The last requirements arise from the magnitude of forces aimed to be measured. The shear moduli of biofilms lie in the range of 100 Pa (untreated biofilm samples) to several hundreds of kPa (*e.g.*, when treated with metal ions). This fact is, on the one hand, important for the choice of the bearing to be used, and on the other hand, important for the choice of the force sensor and the amplifier. They need to be chosen in such a way that the resulting forces from the stretching experiments can be adequately resolved.

**Sample holder and biofilm growth**

One of the key elements in the testing setup is the sample holder for the biofilm samples. This holder has to fulfill several requirements regarding the growth of biofilm samples *in situ*, sample fixation into the measuring setup, and the application of a chemical treatment.

Even though biofilms are able to grow on all kinds of surfaces, growth under laboratory conditions

is usually performed on a solid nutrition layer. The nutrition layer used here is LB agar, a typical growth medium in microbiology, which was also used for all other experiments in this thesis. The LB agar layer ensures that the bacteria are supplied with a sufficient amount of nutrition and can form a continuous biofilm layer. However, a force signal during the stretching process due to the deformation or rupture of the agar layer is undesired. Therefore, it is important that the sample holder consists of two distinct parts, and the biofilm can form a continuous layer over both parts.

The sample holder itself is crafted from PTFE, since PTFE is easy to clean and can be sterilized. This not only renders the sample holders reusable, but also is important to ensure the growth of an uncontaminated biofilm. The sample holder consists of two symmetrical parts, which together form a barbell-shaped trough. The circular cavities at both ends of the sample holder are tapered into narrower, rectangular areas which connect both holder parts. This geometric shape was chosen to keep the agar layer in place during the stretching process. A second feature, *i.e.* a small step in the trough, serves the same purpose (Fig. 2.1). Screws are used to fix the sample holders in the measuring setup.

To prepare the sample holders for the stretching experiment, first the sample holders were cleaned thoroughly and autoclaved. Then, the two parts of the sample holder were brought into contact with each other in a sterile petri dish. The autoclaved, and still liquid agar was poured into the sample holders. After gelation, *i.e.* once the liquid has cooled down, a continuous solid agar layer connected the two sample holders. To ensure that only the biofilm contributes to the force signal during the stretching process, this layer was cut with a sterile scalpel. Afterwards, 15 µL of a liquid overnight culture, as prepared according to biofilm formation protocol *F1*, were spread on the rectangular part of the agar layer with a Drigalski spatula. The sample holders were placed in an incubator at 37 °C for 24 h, after which a continuous biofilm layer formed and stretching measurements could be performed.

**Force sensor**

The force sensor used in this experimental setup is supposed to measure the forces during the stretching process of bacterial biofilms. However, only sparse information can be found in literature about the forces that occur during such an event. An estimation of the forces during the stretching process is necessary to choose a suitable force sensor and amplifier for the setup. As a starting point, the shear modulus of a *B. subtilis* B-1 bacterial biofilm is chosen, *i.e.* $G \approx 100$ Pa, as determined in Section 3.1.2 of this thesis. The shear modulus can be used to calculate the Young's modulus $E$ with the relation:

$$E = 2G(1 + \nu) \tag{3.1}$$

where $\nu$ denotes the Poisson ratio of the material. With the assumption that the biofilm behaves as a homogeneous isotropic incompressible material, *i.e.* $\nu = 0.5$, the Young's modulus of such a material is about 300 Pa. The force $F$ needed to stretch such a biofilm sample is then calculated by

$$F = \frac{E \times A_0 \times \Delta L}{L} \tag{3.2}$$

where $A_0$ denotes the cross section of the sample, $L$ its initial length, and $\Delta L$ the change in length due to the stretching process. Since the rectangular part of the sample holder limits the width of the biofilm during growth, this width, *i.e.* 10 mm, was chosen as the biofilm width. The thickness of biofilms can vary between a few μm and several hundred μm (17), and based on previous experiments with *B. subtilis* B-1 biofilms, 200 μm was chosen as an estimated height for the biofilm samples. These values are used to estimate $A_0$. The initial length of the biofilm samples is very small since the biofilm is grown over a sliced agar layer with the two layer parts touching each other. Thus, moving the stage in the μm range will rapidly result in very high strains of 100 % or more. Therefore, a strain of 100 % was chosen as an initial value for the force estimation. These assumptions lead to an estimated force in the mN range. Based on this estimation, a s-shaped force sensor with a maximal loading force of 2 N (KD-40S 2N, ME-Meßsysteme GmbH, Hennigsdorf, Germany), connected to a 24-Bit amplifier (GSV-2, ME-Meßsysteme GmbH, Hennigsdorf, Germany) was chosen. With this setup, a force resolution of less than 1 mN can be achieved, which should be sufficient to resolve the forces occurring during a stretching test of a biofilm sample.

**Air-bearing and sample movement**

The horizontal installation of the measuring setup offers the advantage of treating biofilm samples right before or even during the stretching process. However, this introduces disadvantages, *i.e.* the need for some kind of moveable support for the sample holder to eliminate lateral forces on the force sensor. As such a support, usually some kind of bearing is used, and the simplest option would be a ball bearing. Even though ball bearings are a common type of bearing, they are limited in their use for precise measuring setups. This is mostly due to the fact that those types of bearings introduce friction in the moving direction, which directly results in additional noise in the force signal. In principle, the noise introduced by this friction can be determined and subtracted from the force signal afterwards. However, this would lead to a lower signal-to-noise ratio of the measuring setup. In comparison to ball bearing types, an air-bearing offers advantages with respect to the requirements for the stretching device. One advantage is that the coefficient of friction is about 2–3 orders of magnitude lower than for ball bearings. Another advantage is that the air-bearing generates an air-film between the static and the moving parts of the measuring setup. As a consequence, stick-slip effects do not occur and the static friction equals the dynamic friction in such bearings. This is crucial as the relative influence of friction is very high when low stretching/rupture forces are to be measured. As the expected deformation of biofilm during the stretching process will be rather large, an air-bearing with a travel distance of 100 mm was chosen. The chosen air-bearing (IBS Precision Engineering BV, Eindhoven, The Netherlands) consists of a case containing a porous material through which pressurized air is pumped, and a moveable bar in the center of this case. The center bar of the bearing rests on an air cushion, weighs approximately 264 g, and can slide horizontally with almost no friction. The pressurized air to generate the air cushion needs to be filtered and dried before it can enter the air-bearing. This is achieved with standard oil removal and filter components for pressurized air, which remove particles down to sizes of 1 μm, and dry the air

prior to injection into the bearing (Parker Hannifin Manufacturing Limited, Gateshead, United Kingdom). To control the movement (and therefore the strain) of the biofilm sample, a Colibri-L LE17 (GUNDA Electronic GmbH, Friedrichshafen, Germany) linear stage is used. This stage offers a precision of ~1 µm, a travel distance of 100 mm, and travel speeds of up to 300 mm/s. The whole setup is mounted to a breadboard to align and fix the parts of the stretching setup.

**Image acquisition**

To follow the rupture process visually, the stretching experiment is recorded with a digital camera (Flea3, Point Grey, Richmond, Canada). This industrial USB 3.0 camera is equipped with a CMOS sensor and is able to capture 60 fps with a resolution of 2080x1552 pixels. The raw data is buffered and processed by the manufacturer's software FlyCapture 2. The resulting movie is directly converted with an H.264 codec to reduce the amount of space needed for storage of data. A high resolution varifocal lens with a focal length between 9 and 90 mm is used (Edmund Optics GmbH, Karlsruhe, Germany) to focus the images.

### 3.2.2 Data analysis

**Filter design**

A key challenge, and at the same time a key requirement for the setup, is the measurement of the forces that occur during the stretching of bacterial biofilm samples. The expected force signals during this process will be very low, *i.e.* close to the lower limit of the force sensor. Another challenge is that the signal will be measured while the linear stage is moving: moving parts typically introduce noise, especially when the force sensor itself is moved. Therefore, the acquired signal has to be adequately filtered to be able to distinguish stretching forces from noise. To reduce noise in a signal, a common way is to apply a filter to the signal. As rather slow changes are expected during the stretching process itself, low-pass filters will be applied and evaluated to filter out high frequency noise in the force signal.

In principle, there are two possibilities to filter a signal. The first one is to filter the signal in real-time, *i.e.* by using an analog filter. The analog filter is advantageous since a time-consuming mathematical post-processing of the signal is not necessary. However, the design of such a filter with resistors and capacitances is difficult, and it has to be adjusted to the other components of the measuring setup. If one of the components, *e.g.* the force sensor is changed, a new filter has to be designed and tested. Such a change of the force sensor could easily be necessary if higher forces are to be expected, *e.g.* due to a stiffening of the biofilm matrix after exposure to metal ions (as measured for the shear modulus in the macrorheological assay, Fig. 3.4), or if other, potentially harder, materials are to be tested. Another option to filter noise is post-processing of the signal with a digital filter. In that case, the signal is recorded and afterwards treated with a filter algorithm. Digital filters can be optimized more easily and faster than analog filters, and thus allow more flexibility in the stretching setup. Therefore, three digital filter variants were taken into account for the measuring setup, *i.e.* a moving average filter

and two frequency domain filters.

The moving average filter is one of the simplest filters possible, and filtering is performed in the time-domain. Filtering is achieved by calculating the average of a selected number of data points. Here, the actual value *x(t)* is replaced by the average of the last 10 data points ($x(t) = \frac{1}{10} \sum_{i=0}^{9} x(t-i)$) of the acquired force signal. This filter is a typical low-pass filter, and the more elements are considered for calculating the average, the smoother the signal becomes. However, fast changes in the signal will then be increasingly suppressed as well. Another option of digital filtering can be performed in the frequency domain, which requires the signal to be first transformed into the frequency domain. Then, well defined cutoff frequencies can be chosen, and specific frequency components are suppressed. The signal is transformed back to the time domain after the filtering process and can be used for further analysis. For the setup, filters with cutoff frequencies $f_{c\,1.5}$ = 1.5 Hz and $f_{c\,3}$ = 3 Hz were chosen for further evaluation.

The raw data of an acquired signal from the force sensor during a stretching process is depicted in Figure 3.10A. However, the signal is very noisy and details are hardly visible. As expected, the movement of the linear stage introduces lots of high-frequency noise into the signal. However, after application of the respective filters, the underlying biofilm-based features become more pronounced and high-frequency noise is successfully suppressed. All three filters show a similar signal shape, but most residual noise is found in the signal filtered with the moving average filter. As expected, the filter $f_{c\,1.5}$ results in an even smoother signal than data treated with $f_{c\,3}$. To take a closer look at the different filters, the step response (mimicking the abrupt onset of the recorded force signal at the initiation of the stretching measurement) can be compared. The response of each filter is depicted in Figure 3.10B on the right side. Here, the low cutoff frequency of $f_{c\,1.5}$ results in a slow signal response to the fast change at the input and overshooting oscillations are generated by the transformation back to the time domain. The moving average filter does not introduce such oscillations, but responds slower and shows more residual noise than the filter $f_{c\,3}$. Therefore, the latter is chosen for data processing since it offers a good trade-off between a fast response on the one hand and a minimization of overshooting oscillations on the other hand.

**Drift correction**

As a next step, example measurements were conducted and the signal was analyzed to decide which signal features can be used to extract parameters describing material properties of biofilms. The force signal of such an example measurement with natively grown *B. subtilis* B-1 biofilms is depicted in Figure 3.11. The blue curve represents the data of a stretching process of biofilm, filtered with the frequency domain filter and a cutoff frequency of 3 Hz as described above. The starting and the end point of the measurements can easily be determined, since the noise, generated by the movement of the linear stage, is clearly visible. Therefore, measurements from different experiments can easily be compared, and the recorded force curves of different experiments can be aligned according to this starting point. To verify that the measured force signal actually depicts the force that is needed for
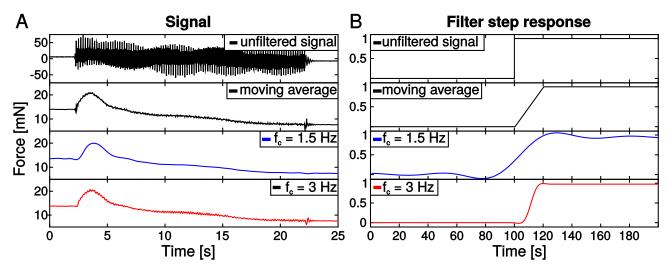
Figure 3.10: **Evaluation of different filters:** (A) A force signal during a biofilm stretching experiment is treated with (black curve) a moving average filter, a frequency domain filter with a cutoff frequency of (blue curve) $f_{c\,1.5} = 1.5$ Hz and (red curve) $f_{c\,3} = 3$ Hz. (B) The response of the respective filters to a step signal at the input.

biofilm stretching, the experiment was repeated with the very same sample. This second time, the biofilm has already been ruptured and therefore no force should be measurable during the stretching process. However, a slight decrease in the force signal could be observed (Fig. 3.11, black curve). This decline arises from the weight of the air-bearing because it is not supported at both ends. Instead, the bar of the bearing moves horizontally along a fixed center case, which causes a slight mass imbalance. Thus, a small pushing force on the force sensor is measured. With increasing travel distance, the center of mass of the central bar moves further and induces an increasing pushing force. On top of this small decline in the force curve, also inertia effects from the acceleration and deceleration of the mass of the measuring setup can be seen in this curve. As this erroneous force signal is highly reproducible and represents the noise of the force sensor in an empty measuring setup, this signal can be used as a reference curve for later measurements. The differences in the initial force detected right before the start of the stretching process arise from stresses induced by the fixation of the sample holder in the measuring setup. However, these initial stresses should not influence the rupture stress of the biofilm and thus can be treated as a simple offset of the force signal during measurement initiation.

To obtain a corrected signal for biofilm stretching (Fig. 3.11, red curve), the reference signal is subtracted from the originally measured force signal. The general shape of the curve is not changed by this correction. Clearly, the biofilm can withstand large strains during the stretching process. This can also be verified when the stretching experiment is followed visually with the mounted digital camera. Two top view images, acquired at different time points of the stretching experiment, are shown in the inset of Figure 3.11. They show that the biofilm is a very soft material: after a stretching distance of 1 mm, most of the biofilm material is still intact and only a small part in the middle of the biofilm is ruptured. In contrast, at a stretching distance of 6 mm, the biofilm is ruptured almost over the full width of the sample, and only small biofilm strings connect the two sample holder parts. However, at this
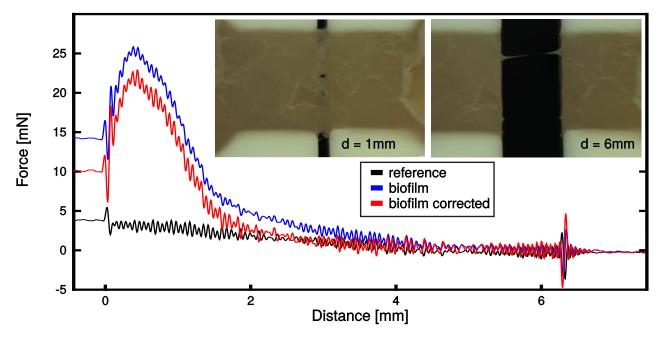
Figure 3.11: **Correction of a force signal:** (blue curve) A force signal obtained for a stretching experiment is corrected with (black curve) a reference signal obtained for the very same sample in a second measurement with the biofilm already ruptured. (red curve) The corrected signal is calculated by subtracting the reference from the force signal. The insets depict a biofilm sample during the stretching process at different strains.

time point only very small forces occur which cannot be distinguished from noise anymore.

**Strain field determination**

So far, it was shown that it is possible to extract force curves corresponding to the biofilm stretching process from the measured force signal. However, it is not clear whether the observed forces are solely arising from the stretching process itself, or if the biofilm detaches from the agar surface during the experiment. If the biofilm would be completely lifted off the substrate, the cohesion forces of the biofilm would be underestimated. Therefore, the movies captured during the experiments were used to calculate an optical flow field of the deformation process. This optical flow field shows the movement of each pixel between a sequence of frames, and thus determines the movement of the biofilm segments during the stretching process. If the biofilm remains adhered at all times of the experiment, mainly biofilm parts that span the agar gap would be deformed. In contrast, if the biofilm would show substantial deformation outside that gap, this would indicate a detachment of the biofilm from the underlying agar layer.

The script used for determining the optical flow is based on the classical optical flow formulation of Horn and Schunck, however modified by a non-local term for integrating flow over large spatial neighborhoods (61). The flow fields of two different biofilm samples were calculated and the results are depicted in Figure 3.12A+B. The calculated flow fields clearly show that the biofilm remained attached
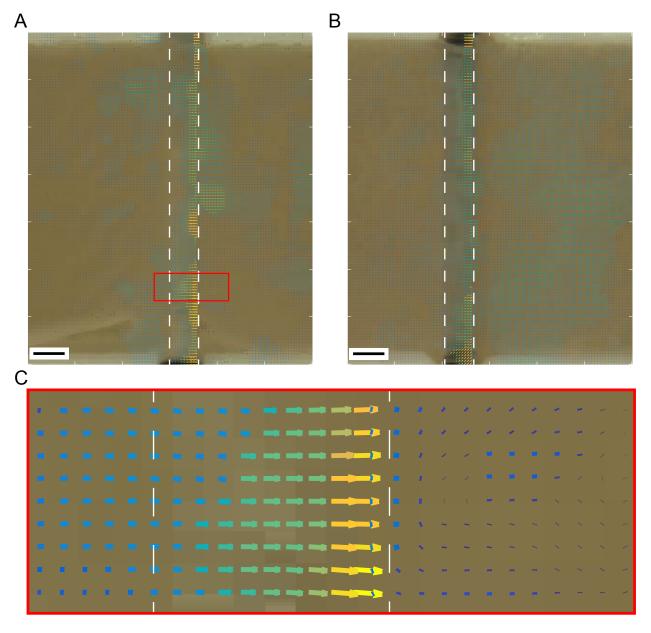
Figure 3.12: **Strain fields of bacterial biofilms:** (A+B) Strain fields of two samples of *B. subtilis* B-1 biofilms during the stretching process. (C) Magnification of the strain field indicated by the red box in A. Dashed lines indicate the edges of the underlying agar layer. Scale bar is 1 mm.

to the substrate layer at all times. Thus, the extracted force curves can indeed be used to determine typical material properties relevant for tensile testing, *e.g.* the tensile strength or rupture energy.

### 3.2.3  Measurements

**Tensile strength of bacterial biofilms**

In the previous part of this chapter, it was shown that it is possible to determine the forces occurring during biofilm stretching with the tensile testing setup. As a next step, quantitative material properties will be extracted from the force curves, and the acquired data will be compared to that from other testing setups. A material parameter which has already been reported in literature for bacterial biofilms is the tensile strength (62), *i.e.* the maximum tension force a material can withstand. The tensile strength is calculated as $\tau = \frac{F}{A_0}$, where $F$ is the force and $A_0$ the cross-sectional area of the sample. In Section 3.2.1, the thickness of bacterial biofilms was estimated to be 200 µm. However, this thickness may vary and depend on the growth conditions (time, temperature) and the availability of nutrients from the nutrition layer beneath the biofilm. Therefore, the thickness was determined for biofilm samples grown in the sample holders. Biofilm samples were grown as described in Section 3.2.1 and cut with a scalpel, to investigate the thickness with an upright light microscope. An example of such an image is shown in the inset of Figure 3.13. The images were evaluated and an average thickness of 300±60 µm was determined, which agrees well with values in literature (17) and the previous estimation. With this thickness value, the cross-sectional area can be calculated and used for the determination of the tensile strength. However, when measurements with biofilm samples were performed more often, a second peak in the force curve appeared (Fig. 3.13). The first, and higher peak, was found to be very reproducible and occurred at identical positions during the stretching process, *i.e.* directly after the start of the movement with the linear stage. This lead to the notion that this peak arises not from the biofilm itself, but from the agar layer beneath. Since the sliced agar layers touch each other after the sample holders are mounted to the measuring setup, the two layers could weakly bind to each other. When the stretching process is started, the two layers are immediately separated and might generate the observed signal peak. To test this notion, further experiments were conducted with sample holders carrying a sliced agar layer only, *i.e.* without biofilm on top. The preparation procedure was performed as described earlier, and after incubation at 37 °C for 24 h, the agar seems to become somewhat sticky. Indeed, a highly reproducible force peak directly after the beginning of the stretching process was recorded with these samples. This 'agar peak' occurred at significantly smaller separating distances than the later 'biofilm peak' (Fig. 3.13), which allows to clearly distinguish those two features. To determine the tensile strength of *B. subtilis* B-1 biofilms, the experiments were repeated with biofilm samples, and the average peak height of the 'biofilm peak' was measured to be 39±11 mN. Taken into account the variations in the thickness of biofilms, the average tensile strength of the biofilm samples was 13±8 kPa. These results agree well with literature values, obtained with other biofilm-forming bacteria, although different testing setups were used for those experiments (62, 63).
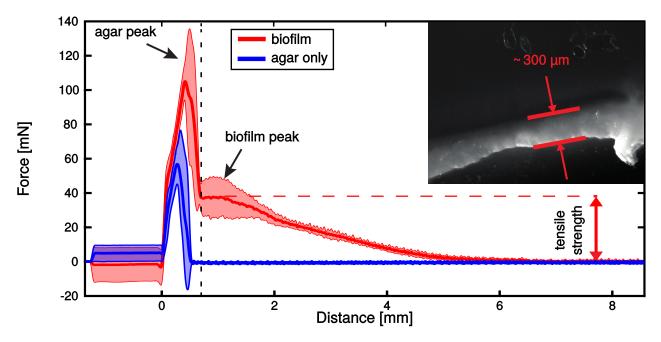
Figure 3.13: **Tensile strength determination:** A stretching process with only a sliced agar layer (blue curve) generates a peak at the onset of the measurement. The two peaks occurring during a stretching experiment with biofilm can be separated into an 'agar peak' and a 'biofilm peak' (red curve). The inset shows the thickness of a bacterial biofilm as determined with an upright light microscope.

### Influence of metal ions on the tensile strength of biofilms

As shown in Section 3.1.3, experiments with *B. subtilis* B-1 biofilms have revealed that the shear stiffness of the biofilm matrix increases after exposure of the biofilms to certain metal ions. Therefore, one might also expect an increase in tensile strength upon biofilm treatment with those metal ions. To test this hypothesis, biofilm samples treated with solutions containing $FeCl_3$ or $CuCl_2$ were tested in the stretching setup. The samples were prepared as described before, and mounted into the testing setup. Afterwards, the fully grown biofilms were treated with a 150 mM solution of $FeCl_3$ or a 150 mM solution of $CuCl_2$ for 30 minutes. The ion solutions were removed with a pipette after the incubation time, and the stretching process was started. As expected, the force curves obtained for treated biofilm samples significantly differed from those of untreated samples (Fig. 3.14). The peak height for biofilm samples treated with $Fe^{3+}$ ions or $Cu^{2+}$ ions was about one order of magnitude higher, and also the peak width differed from that of untreated samples. In detail, the maximum force for biofilm samples treated with $Fe^{3+}$ ions was $175\pm34$ mN and $152\pm25$ mN for samples treated with $Cu^{2+}$ ions, respectively. The treated biofilm samples behaved more brittle, became fully separated at smaller deformations , and showed less necking. As a second parameter, the total energy required to fully separate biofilm samples was calculated. This is achieved by integrating the force signal obtained during the stretching process. To account for the aforementioned 'agar peak', a separation distance of $d$=0.72 mm was chosen as a starting point for integration, and the endpoint was set to $d$=8.57 mm. The obtained rupture energies for the treated biofilm samples were 4–5 fold higher than for the untreated
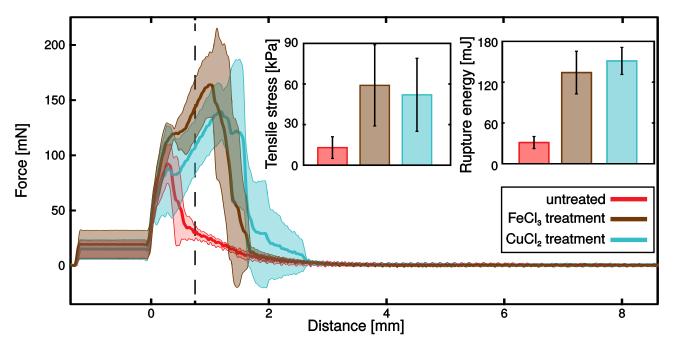
Figure 3.14: **Influence of metal ions on tensile strength:** Force curves obtained for untreated biofilm samples (red curve), and biofilm samples treated for 30 minutes with a 150 mM solution of FeCl$_3$ (brown curve) and CuCl$_2$ (blue curve). The insets depict the corresponding tensile stresses and rupture energies for the samples.

samples (Fig. 3.14, inset). These results correspond well with the measured increase in the tensile stress of treated biofilm samples (Fig. 3.14, inset).

**Influence of strain rate on tensile strength of biofilms**

As biofilm comprises different biopolymers which are transiently cross-linked, also the applied strain rate should have an influence on the tensile strength. This is based on the fact, that the force required to break a transient molecular bond increases with the force loading rate (64). A similar behavior should therefore be observed during biofilm stretching. As a next step, experiments with different strain rates, *i.e.* different velocities during the stretching process, were carried out to test this hypothesis. The chosen linear stage covers a broad range of velocities, and three distinct velocities, *i.e.* a low velocity of 0.03175 mm/s, a moderate velocity of 0.3175 mm/s , and a fast velocity of 3.175 mm/s were chosen. However, the obtained results revealed only minor differences in the tensile strength of the tested biofilm samples. The fast velocity showed a small increased tensile strength, whereas no difference could be detected for the moderate and slow velocities (Fig. 3.15). It is important to realize that the biofilm material does not rupture instantaneously, but instead shows a slow and ductile breaking behavior. This behavior is reflected in the increased width of the 'biofilm peaks' with increasing separation speed. Therefore, the rupture energies for the three different velocities were calculated, and indeed, the biofilm absorbed more energy at higher velocities. The rupture energy calculated even increased monotonically with the stretching rate (Fig. 3.15, inset), which confirms the hypothesis.
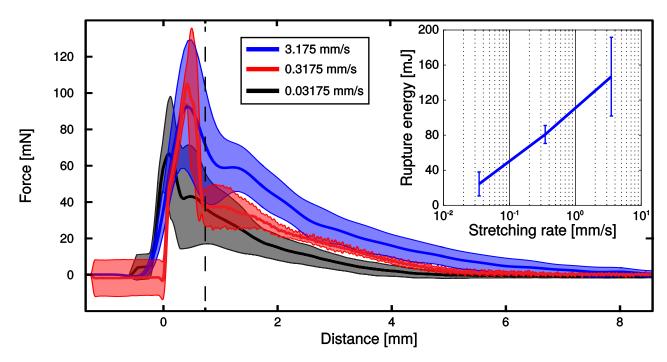
Figure 3.15: **Influence of strain rate on tensile straing:** The experiments were performed with a slow (black curve), a moderate (red curve), and a fast velocity (blue curve). The inset depicts the monotonically increasing rupture energy with increasing stretching rate.

**Multiple stretching cycles**

It is known from literature that biofilms show remarkable self-mending properties (9). Therefore, the applicability of the stretching setup to test the self-healing properties of bacterial biofilm was evaluated in a next step. To test this, it was necessary to adapt the preparation procedure of the biofilm samples, since biofilm samples grown as described so far could not be optimally brought back into contact after biofilm rupture was induced. Therefore, instead of spreading the bacterial liquid culture on the agar surface as described in Section 3.2.1, the liquid culture was now applied to the front sides of the agar layers. Afterwards, the two sample holder parts were fixed to each other with a very small distance (~150 µm, the thickness of a microscopy cover slip) between the two parts. The samples were incubated at 37 °C for 24 h to allow the biofilm to grow over this minimal gap and connect the two agar layers. The force curve obtained for such a biofilm sample did not show an agar peak as observed for the standard biofilm samples discussed before (Fig. 3.16). However, the force curve now contained a pronounced plateau, and the maximum force detected was lower than for the samples measured before. After this force-induced separation, the ruptured biofilm samples were brought in contact for 5 minutes and a second separation of the biofilm was initiated. In the second run, the maximum force was decreased compared to the first run and the plateau disappeared. This was also observed for the third run, where the biofilm strength was substantially decreased and the biofilm ruptured very fast. However, after both runs, the biofilm showed the ability of self-mending, at least to some extent.
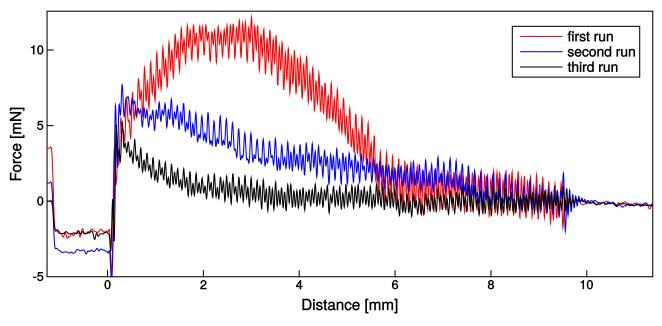
Figure 3.16: **Multiple stretching cycles of biofilm:** Biofilm samples show self-mending properties when ruptured multiple times. Biofilms were brought in contact for 5 minutes after each stretching cycle.

### 3.2.4 Discussion

In this chapter, a new measuring setup to determine the tensile strength of bacterial biofilms was developed. An important feature of this setup is the possibility to measure bacterial biofilms *in situ*. This guarantees that the structural complexity of the biologically grown biofilm material is preserved and not altered by a transfer of the material into the measuring setup. Even though biofilm research crucially depends on quantitative information on the material parameters of biofilms in their unperturbed state, only few dedicated testing setups for such measurements exist (65–67). Measurements of the tensile strength of bacterial biofilms are rare (68–71) even though this material property is important for the development of biofilm removal strategies. The custom-built device developed here allows not only for the measurement of those parameters, but also is able to determine influences chemicals might have on the stretching process. The stretching process can be visually followed during the experiment, and this data can be used to determine the optical flow field of the biofilm samples. Due to the modular design of the setup, multiple samples can be grown in parallel and thus can be measured on the same day. This is advantageous over other setups, where the biofilm is directly grown in the measuring device (66). The setup described here was also modified to perform multi-cycle stretch/relax experiments to study the self-healing properties of biofilms reported before (9). However, to obtain reproducible results of such experiments, the sample holder has to be redesigned in the future. Such an extension of the methodology introduced here could then be applied to test if and how the self-healing properties of bacterial biofilms are altered by chemical challenges.

## 3.3 Matrix composition influence on the material properties of biofilms

In the previous chapters, material properties of *B. subtilis* B-1 biofilms were determined, *i.e.* the shear modulus, resistance to erosion, tensile strength, and the influence of metal ions on all of these properties. Even though these properties are important material parameters and can be used as a basis for, *e.g.* the development of biofilm removal strategies, the results discussed so far only reflect properties of biofilms formed by this particular bacterial strain B-1. Biofilms formed by other bacterial strains may react in a similar way to specific challenges, *e.g.* treatment with metal ions (9, 56, 72–74), but biofilms may also exhibit completely different responses to such challenges. These different responses can be partly attributed to the different environments those biofilms are exposed naturally. The *B. subtilis* species, for instance, can grow in very diverse environments, ranging from the roots of plants (75) to oil fields where the wild-type strain B-1 was found (34). In all those environments, bacteria are exposed to possibly hazardous scenarios, *e.g.* shear forces due to water flow, toxic substances or desiccation, and the biofilm matrix helps to protect the bacteria from them. The underlying mechanisms of how the biofilm matrix achieves such protection are, however, to date not fully understood. It is therefore crucial to obtain a more generalized understanding of the material properties of bacterial biofilms, *i.e.* knowledge about the main molecular components or classes of main components, and their influence on the overall properties of the biofilm. To gather such information about the individual molecular components and their contribution to the overall biofilm properties, knock-out mutants of a bacterial strain can be used. If the matrix composition and the genome of a strain is known, mutants can be developed by knocking out specific genes that are responsible for the production of a particular matrix component. The biofilm matrix produced by such a knock-out mutant then lacks this specific component, but is otherwise identical with the biofilm matrix of the original strain. Such distinct differences in the biofilm matrix composition can then be used to derive conclusions about the purpose of this specific component. Even though the wild-type strain *B. subtilis* B-1 recently has been fully sequenced (76), attempts to generate mutants were unsuccessful so far. This is due to the low transformability of this strain. Therefore, a second wild-type *B. subtilis* strain, *i.e.* NCIB 3610, was chosen to conduct further experiments. The matrix composition of this strain is well studied (2, 36, 37, 77, 78), and knock-out mutants lacking key elements of the biofilm matrix are available. The knock-out strains used in this thesis form biofilms, which each lack one of the following key elements of the NCIB 3610 matrix: the fiber forming protein TasA, the surface protein BslA and the exopolysaccharide EpsA-O. An overview of the knock-out strains and their remaining matrix compositions is given in Table 2.1. These strains will be used in the following chapter to investigate the influence of the matrix composition on a range of different material properties of *B. subtilis* biofilms. The following chapter was mainly adopted from the publication Kesel *et. al*(33).

### 3.3.1 Surface stiffness of biofilms

As a first step, the surface of bacterial biofilms was investigated. The surface of a biofilm is the part of the biofilm, which is exposed to the surroundings, and which represents the barrier between the envi-
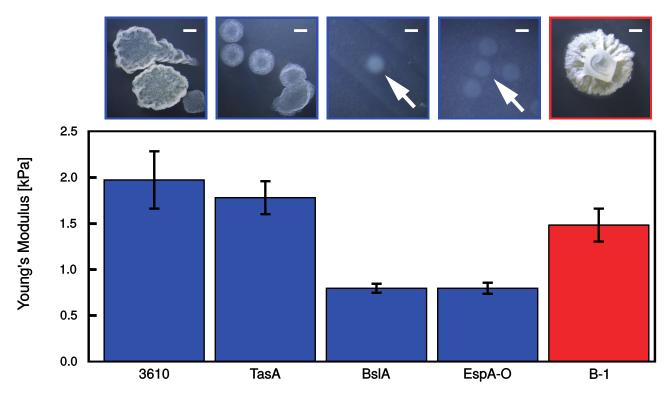
Figure 3.17: **Surface stiffness of different *B. subtilis* biofilms:** The Young's modulus was obtained for one-day-old biofilms of the wild-type strains *B. subtilis* B-1 (red) and NCIB 3610 (blue) and three mutant strains of NCIB 3610 (blue). Error bars denote the standard deviation obtained from at least 9 different samples. Images depict a colony formed by the corresponding strain and the scale bar is 1 μm.

ronment and the bulk material. Therefore, a first material property which was investigated with AFM nanoindentation was the surface stiffness of biofilms formed by the two wild-type strains *B. subtilis* B-1 ($BF_{B-1}$) and NCIB 3610 ($BF_{3610}$), and the knock-out mutants. As biofilms represent a rather soft material, soft cantilevers with a silicone dioxide bead at the cantilever tip were chosen. As a quantitative measure, the Young's modulus was derived with the Hertz model from the retraction curve of the AFM nanoindentation experiments (as described in Section 2.2.9). Initial measurements with biofilms revealed strong electrostatic interactions between the biofilm and the cantilevers when measurements were performed in air. Therefore, a dielectric fluid (99 % ethanol) had to be added to the setup to weaken these effects and obtain reproducible results. In a first experiment, the agar nutrition layer beneath the biofilm was measured and the Young's modulus of the agar layer was calculated $E_{Agar} = 37.82 \pm 5.87$ kPa, which is in good agreement with values found in literature (79). After the stiffness of the agar was determined, $BF_{B-1}$ and $BF_{3610}$ were prepared according to biofilm formation protocol *F2* and the Young's moduli of those biofilms were measured. For $BF_{B-1}$, a Young's modulus of $E_{B-1} = 1.48 \pm 0.18$ kPa was obtained, and the Young's modulus calculated for $BF_{3610}$ was in the same range, $E_{3610} = 1.97 \pm 0.31$ kPa. In a next step, the experiments were repeated with biofilms formed by the previously mentioned knock-out mutants. The notion is, that if a certain key element of the biofilm

matrix is missing and, at the same time, a change in the Young's modulus can be detected, this specific matrix element will be responsible for the observed change of the Young's modulus. When the Young's modulus was determined for the biofilm formed by the TasA knock-out mutant (BF$_{TasA}$), no significant change in the surface matrix stiffness was detected as $E_{TasA}$ = 1.78$\pm$0.18 kPa. In contrast, the Young's moduli decreased by about 50 % when either the protein BslA ($E_{BslA}$ = 0.80$\pm$0.06 kPa) or the exopolysaccharide EpsA-O ($E_{EpsA-O}$ = 0.80$\pm$0.05 kPa) were knocked out from the biofilm matrix. This lead to the notion that both, the protein BslA and the exopolysaccharide EpsA-O contribute to the surface stiffness of the biofilm matrix. However, Kobayashi *et. al*(37) have shown that the production of the surface layer protein BslA of strain NCIB 3610 is dependent on the expression of the epsA-O operon responsible for the production of the exopolysaccharide. Therefore, the decrease in the Young's modulus could be attributed to the absence of the protein BslA in the EpsA-O mutant as well. This hypothesis is supported by the fact that biofilms formed by those mutant strains show an equal decrease in the measured Young's modulus. Since Ostrowski *et. al*(80) showed that BslA is not involved in the synthesis, export or polymerization of the TasA amyloid fibers or the exopolysaccharide, the decrease in surface stiffness of the biofilms formed by the BslA mutant (BF$_{BslA}$) is attributed to the absence of the BslA protein.

### 3.3.2 Surface roughness of biofilms

So far, it was shown that the BslA protein contributes to the surface stiffness of BF$_{3610}$. Hence the question arises, if the surface layer protein is also responsible for changes in other surface properties of *B. subtilis* biofilms. Therefore, as a second surface material parameter, the surface roughness of BF$_{3610}$ and BF$_{B-1}$ was determined with a profilometer (Fig. 3.18A). Indeed, the results showed differences between BF$_{3610}$ and BF$_{BslA}$. BF$_{3610}$ showed a rough surface, whereas the surface of BF$_{BslA}$ showed less roughness features. However, when both those surfaces are compared to the surface profile determined for BF$_{B-1}$, it is clearly visible that BF$_{B-1}$ exhibited an even rougher surface structure with higher peaks (Fig. 3.18A). To quantify the surface roughness, the *Sq* value (see Sec. 2.2.5) was calculated from the surface profiles which confirmed the initial visual impression. The *Sq* value of BF$_{B-1}$ ($Sq_{B-1}$ = 5.5$\pm$3.85) was ~10 fold higher than that of BF$_{3610}$ ($Sq_{3610}$ = 0.53$\pm$0.63). Whereas the lack of TasA in the biofilm matrix showed no significant influence on the measured surface roughness, the surface profiles obtained for BF$_{BslA}$ and biofilms formed by the EpsA-O mutant (BF$_{EpsA-O}$) exhibited a lower roughness than the wild-type strain NCIB 3610 (Fig. 3.18B). This suggests that the surface layer protein BslA is not solely responsible for the surface stiffness, but is also responsible for the surface roughness of NCIB 3610 biofilms. As a next step, the influence of the antibacterial agent ethanol, which was used as a dielectric fluid for the AFM nanoindentation experiments, on the surface roughness was tested. Biofilms were exposed to 99 % ethanol (biofilm treatment protocol *T2*) for 60 minutes and the surface roughness was determined afterwards. When treated with ethanol, the surface roughness of BF$_{3610}$ and the corresponding BF$_{TasA}$ was decreased by ~60 %, whereas BF$_{BslA}$ and BF$_{EpsA-O}$ showed no significant roughness change (Fig.3.18C). The latter finding reflects the fact
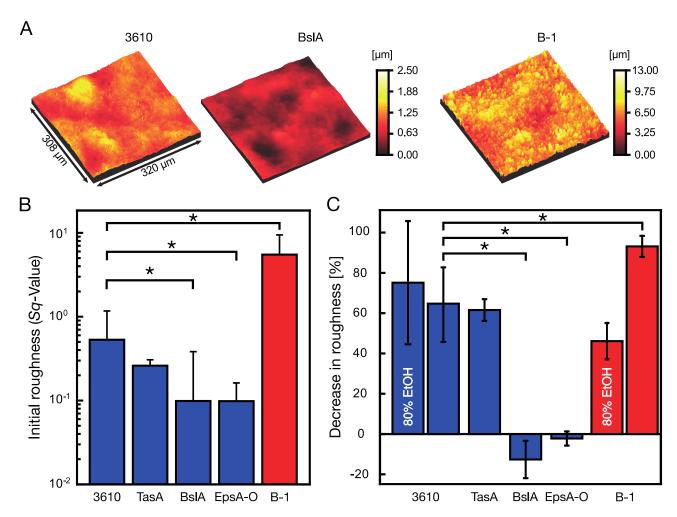
Figure 3.18: **Surface roughness of biofilms:** (A) Surface profiles of $BF_{B-1}$, $BF_{3610}$, and $BF_{BslA}$. (B) Roughness of untreated *B. subtilis* biofilms as quantified by the *Sq* value. (C) Decrease in roughness of *B. subtilis* biofilms after 60 min exposure to ethanol. Error bars denote the standard deviation of 9 samples from 3 different growth batches. * denotes $p < 0.05$.

that the biofilm surfaces of both BslA and EpsA-O mutant strains were found to be very smooth even before ethanol application. $BF_{B-1}$, which possessed the highest initial roughness of all tested strains here is also affected most by the ethanol treatment: more than a 90 % decrease in surface roughness was measured. As typical ethanol concentrations used for disinfection applications are in the range of 70-80 %, the profilometer experiment was repeated for $BF_{B-1}$ and $BF_{3610}$ with a concentration of 80 % ethanol. A similar decrease in roughness was found for $BF_{3610}$, but a lower decrease of ~50 % was found for $BF_{B-1}$ (Fig.3.18C).

### 3.3.3 Viscoelastic properties of biofilms

In the previous experiments, the surface properties of *B. subtilis* biofilms, and the influence of the common disinfectant ethanol on the biofilm roughness were determined. However, such an ethanol
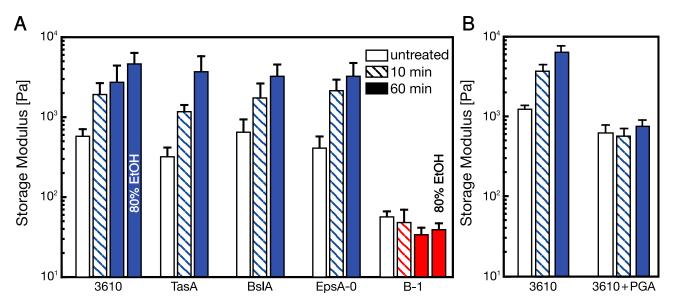
Figure 3.19: **Influence of ethanol on biofilm viscoelasticity:** (A) Storage modulus of $BF_{B-1}$ (red) and $BF_{3610}$ (blue) and biofilms formed by the three mutant strains of NCIB 3610 (blue). (B) Storage modulus of $BF_{3610}$ grown in the absence and presence of γ-PGA. Error bars denote the standard deviation of 9 samples from 3 different growth batches.

treatment may not only alter the biofilm surface, but could also influence the bulk properties of the biofilm material. Results by Epstein *et. al*(6) revealed that $BF_{3610}$ show extreme resistance to wetting with ethanol for concentrations as high as 90 %. Therefore, an 80 % ethanol solution may not even be able to penetrate the biofilm matrix and induce changes in the bulk material properties. Thus, 99 % ethanol was chosen to treat the biofilm samples and compare the viscoelasticity of untreated and ethanol treated biofilm samples. As a quantitative parameter, the storage modulus determined at a frequency of 1 Hz is compared. This simplification is justified since previous experiments showed that the overall shape of the frequency spectra of biofilms were not altered by a chemical treatment of the biofilm (Fig. 3.4).

In a first step, the storage moduli of untreated biofilm samples were obtained with a macrorheometer. The storage modulus measured for $BF_{3610}$ was $G'_{3610}(1\,Hz) = 584 \pm 132\,Pa$, and all biofilms formed by the mutants of this strain had moduli in a similar range (Fig. 3.19A). In contrast, the storage modulus for $BF_{B-1}$ was about one order of magnitude lower (Fig. 3.19A). In a next step, biofilms were treated with 99 % ethanol for 10 minutes as described in biofilm treatment protocol *T2*. Afterwards, the storage moduli were determined and compared with that of untreated biofilm samples. For $BF_{3610}$ and the biofilms formed by the mutant strains, an increase in the elasticity upon ethanol treatment was detected, whereas for $BF_{B-1}$ no significant alteration in the elastic modulus was measured. However, treatments with other chemicals revealed that 10 minutes may not be enough for the chemical treatment to show its full effect (Fig. 3.3). Therefore, the experiments were repeated with a treatment time of 60 minutes. After this longer time span, the ethanol-induced effect on the biofilm elasticity is even more pronounced to what was observed for the short treatment time. The elastic modulus of $BF_{3610}$ and
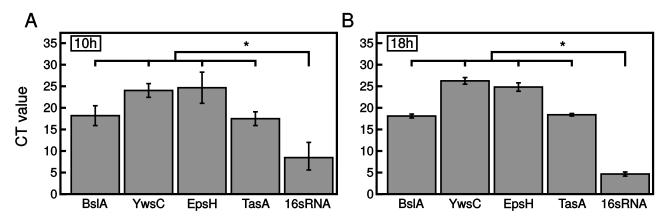
Figure 3.20: **mRNA production of biofilm matrix proteins in BF$_{B-1}$:** Gene expression analysis at (A) 10 h and (B) 18 h of biofilm growth. *B. subtilis* B-1 mRNA production of genes corresponding to matrix components described for strain NCIB 3610 in comparison to the 16S rRNA control was analyzed. Error bars denote the standard deviation obtained from 3 biological and 3 technical triplicates. * denotes $p < 0.05$.

biofilms formed by the mutants was further increased, whereas for BF$_{B-1}$ no significant alteration was detected (Fig. 3.19A). When the experiments were repeated with a lower concentration of ethanol, *i.e.* 80 % ethanol as commonly used for disinfection, the outcome was not significantly changed for BF$_{B-1}$ and BF$_{3610}$ (Fig. 3.19A). Together, these results revealed that changes in the bulk viscoelasticity upon treatment with ethanol occurred for all *B. subtilis* biofilm variants with one exception: B-1 biofilms. If the molecules TasA, BslA or EpsA-O are missing in the NCIB 3610 biofilm matrix, similar changes in the biofilm viscoelasticity are observed as for wild-type NCIB 3610 biofilms. However, different results were obtained for BF$_{B-1}$ and BF$_{3610}$, which leads to the hypothesis, that this difference could be attributed to differences in the composition of the wild-type strain biofilm matrices. Hence, there must be another molecule in the matrix of BF$_{B-1}$ which is responsible for this protection, but is missing in BF$_{3610}$ biofilms.

### 3.3.4   Protection of biofilms by γ-PGA

Information about the matrix composition of biofilms formed by the wild-type strain B-1 is rather sparse, and the biofilm matrix was described to consist mainly of γ-PGA (13). Since the two strains are genetically related, and it is not clear whether the wild-type strain B-1 also secretes key elements of the NCIB 3610 matrix. To test this, a gene expression analysis was conducted and *B. subtilis* B-1 biofilms grown for 10 h and 18 h were analyzed. In this analysis, it was tested whether the genes encoding the matrix components of BF$_{3610}$, *i.e.* TasA, BslA and EpsA-O, are also transcribed in the biofilms formed by wild-type strain B-1. Additionally the gene ywsC, important for the production of γ-PGA was tested, and 16S rRNA was chosen as a housekeeping gene. At both time points of biofilm growth, the gene expression analysis revealed that mRNA of the gene ywsC is indeed produced, although at lower levels compared to the housekeeping gene (Fig. 3.20). Surprisingly, mRNA for the production of BslA,
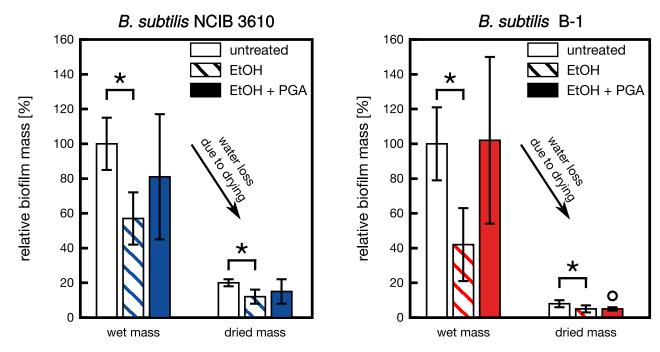
Figure 3.21: **Wet and dry mass of wild-type biofilms:** The wet mass and dry mass (after lyophilization) of $BF_{3610}$ and $BF_{B-1}$ are determined without (empty bars) and with ethanol treatment (striped bars). Addition of γ-PGA during the growth of biofilms protects $BF_{B-1}$ from ethanol-induced dehydration (filled bars). Error bars denote the standard deviation obtained from 3 biological and 3 technical triplicates. Circle indicates that lyophilization process did not always work on this condition. * denotes $p < 0.05$.

TasA and EpsA-O can also be found in the biofilm matrix of strain *B. subtilis* B-1. This is somewhat unexpected and indicates that the B-1 biofilm matrix could also contain key elements of the NCIB 3610 biofilm matrix. This would render γ-PGA the main molecular difference between the two biofilm matrices. Thus, if γ-PGA constitutes the main difference in the matrix composition, it could also be the reason for the different responses of the biofilms upon treatment with ethanol. The observed increase in biofilm stiffness could arise from an ethanol-induced dehydration of the biofilm matrix. γ-PGA is a strongly hygroscopic material when prepared as a powder, thus γ-PGA could prevent a loss of water in B-1 biofilms, which in turn would result in a protection from a stiffening of the biofilm matrix due to ethanol. To test if γ-PGA also protects the NCIB 3610 biofilm matrix from ethanol-induced dehydration and ethanol-induced stiffening, $BF_{3610}$ were grown in the presence of purified γ-PGA, and the macrorheological characterization was repeated. In detail, γ-PGA was extracted from a liquid culture of B-1 (81), and the liquid overnight culture of NCIB 3610 (prepared according to biofilm formation protocol *F2*) was enriched with 4.75 mg/ml of γ-PGA. 100 µL of this bacterial suspension were streaked onto agar plates and incubated at 37° C. When NCIB 3610 biofilms were grown in presence of purified γ-PGA, the storage modulus was slightly decreased compared to normally grown $BF_{3610}$ (Fig. 3.19B). Additionally, the γ-PGA supplementation resulted in a protection of $BF_{3610}$ from an ethanol-induced stiffening of the biofilm matrix, comparable to $BF_{B-1}$ (Fig. 3.19B). So far, it is not clear if ethanol indeed

induces a dehydration of $BF_{3610}$ and if this dehydration leads to the observed stiffening of the biofilm matrix. To test this, the amount of water trapped in the biofilm matrix was determined by measuring the wet and dry mass of both biofilm variants. In a first step, the average mass of the biofilms produced by the wild-type strain B-1 and NCIB 3610 was determined. $BF_{B-1}$ produced a ~4 fold higher biomass (1170 mg/agar plate) than $BF_{3610}$ (303 mg/agar plate). As a second step, the effect of an ethanol treatment on the wet biofilm mass was determined. After ethanol treatment, the wet mass of $BF_{3610}$ was lower by ~40 % and lower by ~60 % for $BF_{B-1}$ compared to the untreated samples (Fig. 3.21). This is somewhat unexpected since the hypothesis was, that γ-PGA protects $BF_{B-1}$ from ethanol-induced dehydration. However, the differences in the wet mass measured so far could also be due to a lower production of biofilm mass on the particular agar plates chosen for ethanol treatment. Therefore, to check whether the measured lower wet mass is indeed due to a loss of water, the samples were freeze-dried, which removes the liquid phase of the samples, and the dry mass was determined afterwards. If differences in the dry mass would be detected, this could have two causes. On the one hand, it could mean that not only water is removed from the biofilm due to the ethanol treatment, but also biomass. On the other hand, it could be that the amount of biomass produced on the selected agar plates was lower in the first place, leading to a lower amount of water stored in the biofilm. Indeed, when the samples were freeze-dried, $BF_{3610}$ and $BF_{B-1}$ showed significant differences in the dry mass between untreated and treated samples (Fig. 3.21). Further analysis of the data revealed that the ratio between wet mass and dry mass is ~5 for $BF_{3610}$ untreated and treated samples. This indicates that the same fraction of water is present in $BF_{3610}$ before and after an ethanol treatment. Yet, this is not the case for $BF_{B-1}$ where the fraction of water stored in the biofilm is higher in the untreated samples than in the treated samples.

In a last step, to determine the influence of γ-PGA on the water content of biofilms, $BF_{3610}$ and $BF_{B-1}$ were grown in the presence of γ-PGA as described previously for the rheological characterization. Afterwards, the biofilms were treated with ethanol and the wet and dry mass was determined. When $BF_{3610}$ was supplemented with γ-PGA during the growth phase, the ratio of wet mass to dry mass was again ~5, as already determined for normally grown $BF_{3610}$ (Fig. 3.21). Therefore, the addition of γ-PGA does not prevent ethanol-induced dehydration in $BF_{3610}$. However, when $BF_{B-1}$ was supplemented with γ-PGA during the growth phase, the ratio of wet mass to dry mass was increased compared to not-enriched $BF_{B-1}$ (Fig. 3.21). Thus, additional γ-PGA prevents ethanol-induced dehydration of $BF_{B-1}$.

### 3.3.5   Discussion

In this chapter, biofilms formed by the two *B. subtilis* strains NCIB 3610 and B-1, were compared regarding their material properties, *i.e.* the surface stiffness, surface roughness, and bulk elasticity. Additionally, 3 knock-out mutants lacking key components of the $BF_{3610}$ matrix were investigated. Key matrix components of the NCIB 3610 biofilm matrix are the fiber-forming protein TasA, the surface layer protein BslA and the exopolysaccharide EpsA-O. In contrast, the matrix of biofilms formed by the strain

B-1 is known from literature to be mainly composed of γ-PGA, which is absent in biofilms produced by strain NCIB 3610. However, gene expression experiments revealed that also key elements of the NCIB 3610 matrix could be present in the B-1 matrix. The polyanionic biopolymer γ-PGA seems to serve a dual role in the biofilm matrix of *B. subtilis* B-1 biofilms. On the one hand, γ-PGA is responsible for a stiffening of the B-1 biofilm matrix. For instance, if exposed to metal ions, the potentially toxic metal ions are trapped in the biofilm matrix through complexation with polyanionic biofilm polymers such as PGA (see Sec. 3.1.6). On the other hand, γ-PGA is responsible for the protection of B-1 biofilms from ethanol-induced changes of the biofilm stiffness. This protection may be partly attributed to the ability of γ-PGA to bind and thus trap water inside the biofilm matrix. Even though the natural occurring concentration of γ-PGA (<0.1 mg/ml (34)) in the B-1 biofilm matrix may be sufficient to keep the bulk elasticity constant after an ethanol treatment, such a low concentration fails to protect the B-1 matrix from ethanol-induced dehydration. However, this dehydration protection can be achieved when strain B-1 is supplied with additional purified γ-PGA during biofilm growth. This supports the hypothesis that the hygroscopic γ-PGA traps water inside the biofilm matrix, since a higher amount of γ-PGA in the biofilm matrix could bind higher amounts of water. However, this water trapping mechanism of γ-PGA cannot be transferred to biofilms formed by the *B. subtilis* strain NCIB 3610. Nevertheless, these γ-PGA-enriched $BF_{3610}$ are protected from ethanol induced stiffness changes of the biofilm matrix. This leads to the hypothesis that the protection mechanism of γ-PGA to prevent a biofilm stiffening is not achieved by trapping water inside the biofilm matrix, but maybe γ-PGA binds ethanol and thus shields the other biofilm matrix molecules from ethanol. The biopolymer γ-PGA is also found in many other *Bacillus* species, *e.g. B. anthracis, B. megaterium, and B. licheniformis* (82), serving a variety of different purposes depending on the strain and the environment, *e.g.* virulence factor (83), or complexation of metal ions (84). Such a multifunctional role as seen here for γ-PGA is also found for other polyanionic polymers in different biofilms. For instance, biofilms formed by *Pseudomonas aeruginosa* contain the polymer alginate which also serves multiple functions in the biofilm matrix. It is important for providing structural stability (26), complexation of metal ions (9) and also is attributed high water binding capacities (27). Furthermore, the data presented here is an example of the ability of bacteria to use externally available molecules for their own good. Similarly, it has been shown that bacterial knock-out strains can be supplemented with the missing biofilm matrix components to fully restore the original biofilm matrix (2, 77). The presented supplementation with γ-PGA shows that bacteria can also incorporate foreign components into their biofilm matrix, *i.e.* even if this particular component cannot be secreted by the bacteria themselves. Another biofilm component, important for the overall biofilm material properties, is the surface layer protein BslA. This protein is mainly responsible for the surface stiffness and surface roughness of the biofilm matrix of $BF_{3610}$. When this protein is missing in the biofilm matrix, not only a decrease in the surface elasticity but also in the biofilm surface roughness can be detected. BslA was also shown to contribute to the extreme wetting resistance of $BF_{3610}$ (6). This hydrophobicity was attributed, at least in part, to the increase in surface roughness of the biofilm. This surface roughness-induced hydrophobicity, or so-called lotus effect, is in the focus of researchers (85), and many attempts are made to transfer this effect to bio-

inspired materials.  Therefore, a further step in biofilm research could be the attempt to transfer material properties of biofilms, *i.e.* hydrophobicity, to artificial materials.  This idea will be covered in the next chapter.

## 3.4 Biofilm-enriched hybrid mortar

In the previous chapters, various material properties of biofilms formed by two different *B. subtilis* strains were investigated and compared. One main result of the investigation was, that the surface layer protein BslA is responsible for the surface roughness of biofilms produced by strain NCIB 3610. However, it is also known from literature that BslA plays an important role in the extreme wetting resistance of $BF_{3610}$ (78). Whereas $BF_{3610}$ shows extreme hydrophobic behavior, biofilms formed by the knock-out mutant of this strain, *i.e.* $BF_{BslA}$, not capable of secreting this surface layer protein, show hydrophilic behavior. Such an extreme wetting resistance is also found on other naturally occurring surfaces, *e.g.* lotus leaves and rose petals. Especially the lotus-effect has been thoroughly investigated (85), and artificial materials mimicking those superhydrophobic and self-cleaning properties have been developed (86). But also other materials and surfaces showing hydrophobic properties are under active investigation (87, 88).

In principle, several possibilities exist how properties of natural materials can be transferred to artificial materials. A first, and probably the simplest approach, could be to mix the two materials of interest, thus creating a hybrid material with the desired properties. However, in such a simple scenario, the hybrid material contains all constituents of the biological material, which could lead to additional but undesired effects in the new material. Thus, a more advanced approach would be to add only the one specific component, which is responsible for the desired mechanism in the natural material, to the artificial material. Yet, this renders the production process of the hybrid material more difficult and time-consuming, since the specific component has to be purified or extracted from the natural material. Such an approach can also be realized with the use of artificial components, which do not rely on natural materials. This includes the modification of an artificial material by adding other artificial components, or a surface treatment of the artificial material after the curing process. However, this is in some cases even more challenging or could include the use of hazardous chemicals, rendering the generation process dangerous.

All those principles mentioned here have been investigated and applied to create superhydrophobic surfaces through coating or mixing approaches (88–91). However, the key goal in the development of hydrophobic materials is often not solely to generate a hydrophobic surface, *e.g.* for the purpose of self-cleaning, but it is many times also desired to prevent or delay the ingression of water into the bulk material. One field in which the latter is critically needed is civil engineering, where cement-based materials typically suffer from water and chloride ingression (92). Water invades the material through microcracks, and freeze-thaw cycles can lead to a macroscopic damage of the material. The ingression of chloride on the other hand leads to corrosion of embedded steel structures, critically reducing their mechanical stability. Therefore, it would be advantageous to render not only the surface of cementitious materials hydrophobic, but also to prevent or delay the ingression of water into the bulk material. Many strategies to date have experimented with surface modification approaches to develop hydrophobic cement (93, 94). Since these strategies require coating the cementitious material, this additional step is time-consuming and costly. This calls for the development of a cementitious material
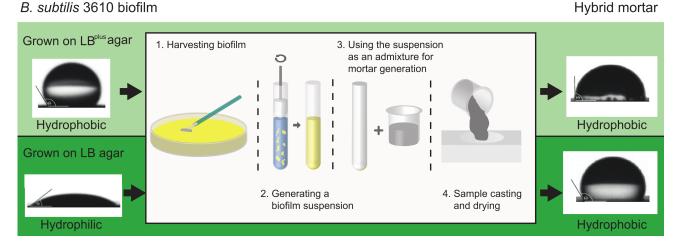
Figure 3.22: **Schematic of the production process of hydrophobic hybrid mortar:** When either hydrophilic or hydrophobic biofilm variants are added during mortar generation, the resulting hybrid mortar shows an overall hydrophobic behavior.

with a simple production process. Ideally, this process would not be limited to a surface modification. It will be shown in the following chapter, that the addition of biofilm material during the mortar casting process achieves a bulk modification of the mortar material, which leads not only to a hydrophobic surface but to a strong delay of water ingression into the hybrid material compared to standard mortar.

### 3.4.1   Influence of biofilm addition on the hydrophobicity of mortar

A first step towards the investigation of hydrophobic properties of hybrid mortar is to measure the static contact angle of a water droplet. This is achieved by placing a drop of ddH$_2$O on the surface of the mortar material, and determine the angle at the 3-phase-junction between the solid surface, the water droplet and the surrounding gas. A high level of hydrophobicity correlates with a high contact angle. Contact angles below 90° represent a hydrophilic, thus wettable surface whereas materials with contact angles above 90° are called hydrophobic. Surfaces with contact angles above 120° are sometimes referred to as superhydrophobic.

In a first experiment, the hydrophobicity of BF$_{3610}$ grown according to biofilm formation protocol *F1* was measured. When grown on LB agar, the biofilm formed by *B. subtilis* strain NCIB 3610 showed an overall hydrophilic behavior with contact angles in the range of 30–40°. However, when grown on a different medium, biofilms formed by this strain indeed show hydrophobic behavior (6). Since it may be a reasonable assumption that a hydrophobic additive is needed to obtain a hydrophobic hybrid mortar, a different medium was chosen for biofilm formation so that a hydrophilic biofilm is obtained. When LB was enriched with a combination of glycerol and manganese, biofilms formed by strain NCIB 3610 became hydrophobic with contact angles of about 110°. Additionally, this enriched medium promotes biofilm formation in the *B. subtilis* species (95) which yields an increased output of biofilm mass. This enhanced biofilm production also facilitates the experiments since less LB agar plates have to be
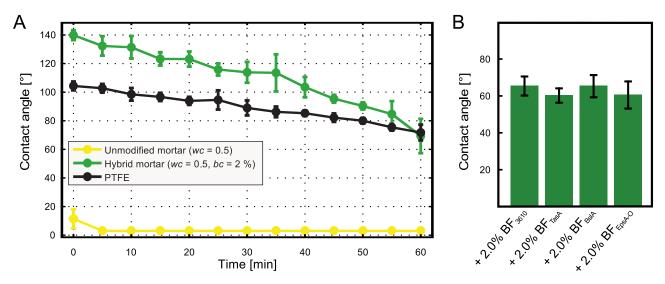
Figure 3.23: **Contact angles of water droplets on hybrid mortar:** (A) Wetting resistance of unmodified mortar compared with a PTFE sample and a hybrid mortar sample: the contact angle of a given water droplet is followed over a time span of 60 minutes. (B) Comparison of different biofilm mutants used as admixtures to generate hybrid mortar samples.

harvested to generate the hybrid mortar samples.

To investigate whether the addition of such a hydrophobic biofilm material could render simple mortar hydrophobic, the biofilm was added during the mortar casting process (Fig. 3.22). In detail, biofilm was harvested from agar plates by manual scraping. Afterwards, the biofilm material was mixed with water and homogenized using a pestle to generate a liquid suspension. This suspension was mixed with cement and sand to create hybrid mortar. When 2 % of biofilm ($w_{\text{wet biofilm}}/w_{\text{sand + cement}}$) was used in the liquid suspension to create the hybrid material, the contact angle was ~90 °, whereas for a normal, unmodified mortar the contact angle is in the range of 30 °. This shows, indeed, that the addition of hydrophobic biofilm to standard mortar yields a hydrophobic hybrid material. However, it is unclear whether the increased wetting resistance is based on the addition of a hydrophobic biofilm component, or on the addition of the biofilm material itself. To test this, the experiments were repeated with biofilms formed by mutants of strain NCIB 3610 which were already used in the previous chapter. If the hydrophobic key component BslA would be responsible for the hydrophobicity of the hybrid mortar sample, the addition of $BF_{\text{BslA}}$ as an admixture would result in a hydrophilic hybrid mortar, whereas all other biofilms would still yield a hydrophobic hybrid mortar. Surprisingly, when the hybrid mortar samples were prepared with biofilms formed by the mutant strains, the determined contact angles showed no significant differences compared to samples generated with the wild-type strain (Fig. 3.23B). This shows that neither the hydrophobic component of the NCIB 3610 biofilm, *i.e.* the surface layer protein BslA, nor the other key elements of the biofilm matrix are responsible for the hydrophobic properties of the hybrid material. Hence, the question arises whether a hydrophobic biofilm is needed to achieve a hydrophobic hybrid material. To test this, $BF_{3610}$ was grown on the simple LB medium which results in a hydrophilic biofilm. This biofilm was then used to generate
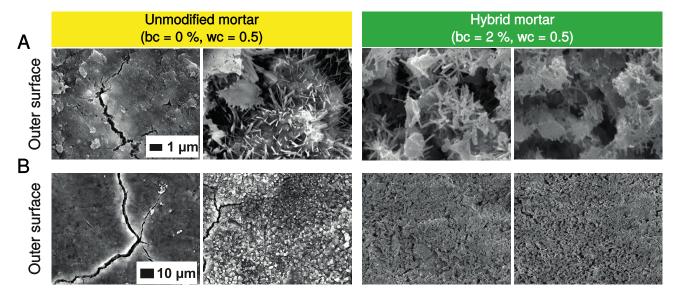
Figure 3.24: **SEM images of unmodified and hybrid mortar samples:** Hybrid mortar samples show a higher density of ettringite-like crystals on the surface than unmodified mortar samples. The 1 µm scale bar applies to all images in A, whereas the 10 µm scale bar applies to all images in B.

the hybrid mortar material and the wetting resistance was determined. When this hydrophilic biofilm was added, the contact angle measured on the hybrid material reached similar or sometimes even higher values compared to when hydrophobic biofilm was added (Fig. 3.22). This result shows that the increased wetting resistance does not directly arise from the hydrophobicity of the added biofilm. Instead, the structure of the mortar material might be affected due to the addition of biofilm. One notion, based on the fact that hydrophobic behavior can also be induced by surface roughness is, that the addition of biofilm leads to an increased surface roughness of the hybrid material and thus to an increased wetting resistance. This idea is tested in the next section.

### 3.4.2   Surface roughness of hybrid mortar

Well-known examples of natural surfaces with roughness-induced hydrophobic properties are the lotus-leaf and rose-petals (85). Such a surface roughness-induced hydrophobicity could also be the mechanism responsible for the increased wetting resistance of the hybrid mortar samples. To investigate if the surface structure of mortar is altered by the addition of the biofilm material, the surface of the mortar samples was visualized using scanning electron microscopy (SEM). Indeed, a high density of elongated spike-like structures was observed on the surface of the hybrid mortar samples (Fig. 3.24). An explanation what the observed spikes could be is that these are the bacteria added together with the biofilm. However, these spike-like structures are also found on the unmodified mortar sample, albeit at only a few spots. In fact, these structures look like typical ettringite-like crystals as they are observed during the casting of Portland cement (96). The high density of those spike-like structures leads to an increased roughness of the surface and thus supports the hypothesis of a roughness-induced hydrophobicity of the hybrid mortar samples. A drawback of the SEM technique is that a calculation of

Unmodified mortar
$Sq$ = 2.56±0.81 µm
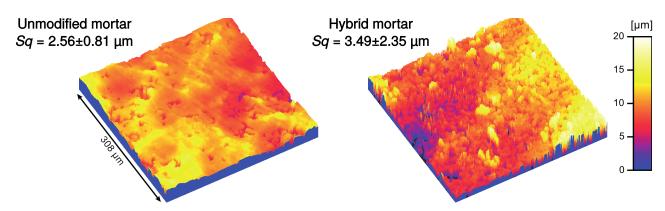
Hybrid mortar
$Sq$ = 3.49±2.35 µm

[µm]

308 µm

Figure 3.25: **Light profilometer images of unmodified and hybrid mortar samples:** Hybrid mortar samples show increased surface roughness compared to unmodified mortar samples.

roughness parameters from SEM images is not possible. However, to quantitatively compare the surface roughness of hybrid mortar and unmodified mortar, such parameters are necessary. Therefore, the surface was investigated with a light profilometer, as with this technique, quantitative parameters describing the surface roughness, *e.g. Sq* can be determined. When the surface profiles of unmodified mortar and hybrid mortar were compared, the visual impression that the surface of hybrid mortar is rougher was quantitatively confirmed. The calculation of the $Sq$ value revealed a roughness of the unmodified mortar sample of $Sq$ = 2.56±0.81 µm whereas the hybrid mortar possessed a value of $Sq$ = 3.49±2.35 µm (Fig. 3.25).

These results clearly demonstrate that the addition of bacterial biofilm leads to an increased surface roughness of the hybrid mortar samples. However, it is not clear whether the surface structure as determined by profilometry indeed contains biofilm material or if the material is solely composed of the mortar components, *i.e.* cement, sand, and the products of the hydration reaction. Therefore, a XPS analysis was performed, and the obtained spectra for unmodified mortar, hybrid mortar, and biofilm produced by strain NCIB 3610 were compared to confirm the presence of biomatter in the hybrid mortar sample. Since nitrogen is an abundant element present in bacteria and the biofilm matrix, but missing in both cement and sand, the spectra are examined for the presence of such a nitrogen peak. Indeed, this peak was pronounced in the spectra of the biofilm material and the hybrid mortar material, whereas no peak is observed in the unmodified mortar sample (Fig. 3.26). Thus, the presence of this nitrogen peak leads to the conclusion that biofilm material can be found at the surface of the hybrid mortar samples.

### 3.4.3 Influence of the hybrid mortar composition on the contact angle

So far, it was shown that the addition of biofilm to standard mortar leads to an increased surface roughness and thus to an increased wetting resistance of hybrid mortar samples. Up to now, the biofilm content of the hybrid mortar samples was kept constant for all samples. However, the amount of added biofilm material might correlate with the wetting resistance of the hybrid mortar. To test this, mortar samples with increasing amounts of biofilms were prepared and the contact angles were measured.
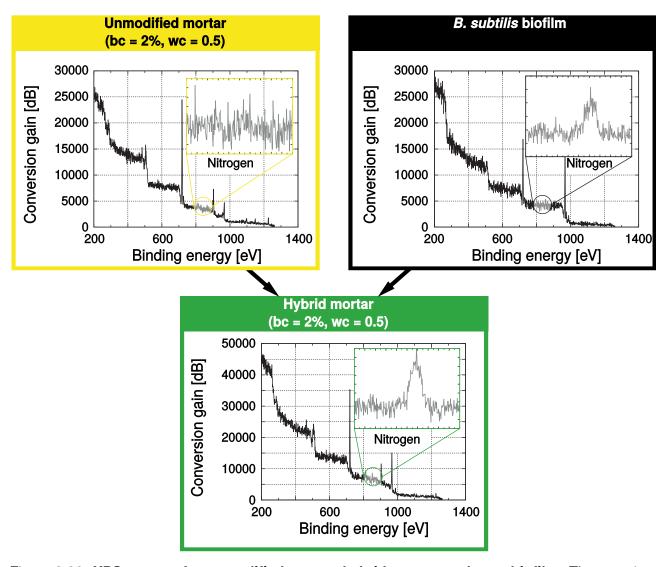
Figure 3.26: **XPS spectra for unmodified mortar, hybrid mortar, and pure biofilm:** The overview spectra show all characteristic elements present in each sample. The nitrogen peak (840–860 eV) in the high resolution spectra is present in the biofilm and hybrid mortar sample but not in the unmodified mortar sample.

The results show that also the wetting resistance for a biofilm content of 1.0 % was increased compared to the unmodified mortar sample (Fig. 3.27). If the biofilm content was stepwise increased to 2.5 %, the contact angles gradually increased (Fig. 3.27). Yet, when even higher amounts of biofilm mass were added to the mortar mix, the hybrid mortar crumbled easily and could not be cast into a rigid sample anymore. The properties and workability of standard mortar typically depends on the amount of water which is used to generate the material (97). The so called water/cement ratio (wc) is usually in the range of 0.5 to 0.7 (98), and is defined as the ratio of the weight of water added to the weight of cement during the mixing process. To test the influence of an increased wc on the hybrid mortar samples, the biofilm content was kept constant at 2.0 % while the wc was gradually increased to 0.6 and 0.7. The
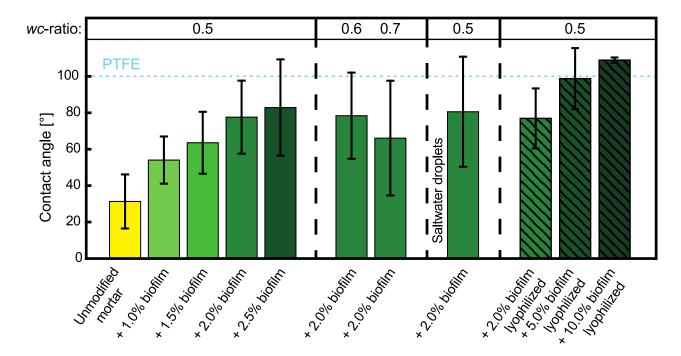
Figure 3.27: **Influence of the hybrid mortar composition on the contact angle:** Higher amounts of biofilm lead to an increased wetting resistance of hybrid mortar samples up to 2.5 % (w/w) biofilm content. When the water/cement ratio is increased, the wetting resistance slightly decreases. The contact angle for saltwater (600 mM NaCl) is comparable to that obtained for ddH$_2$O. In lyophilized form, larger amounts of biofilm can be added to the mortar, which leads to even higher contact angles of the hybrid mortar samples.

additionally added water only entails a minor decrease in the measured contact angles (Fig. 3.27). As mentioned before, chloride ingression into cementitious materials is a major factor affecting their durability (99). Such a chloride ingression commonly occurs during winter time, when splash water containing salt is swirled by cars onto mortar structures. Moreover, also mortar structures exposed to seawater environments suffer from chloride ingression, which lead to corrosion of the embedded steel structures, thus critically reducing their stability. To test if the hybrid mortar samples also show an increased wetting resistance to saltwater, droplets of a 600 mM NaCl solution were used to determine the contact angles. Hybrid mortar samples showed similar resistance towards wetting with saltwater droplets as towards ddH$_2$O, which demonstrates a high potential of the hybrid mortar for industrial usage.

However, for a convenient industrial application, the process of creating the samples is still too complicated and time-consuming, since fresh biofilm has to be harvested directly prior to creating the hybrid mortar samples. Furthermore, the grinding process of the biofilm to create a liquid biofilm suspension is a second time-consuming step in the production process. One idea to simplify the mortar generation process would be, to use a storable biofilm powder as an admixture. Such a biofilm powder can be easily produced by freeze-drying fresh biofilm, also rendering the biofilm material storable for later usage. When 2 % of this powder (equivalent to 2 % fresh biofilm mass) was used to create the
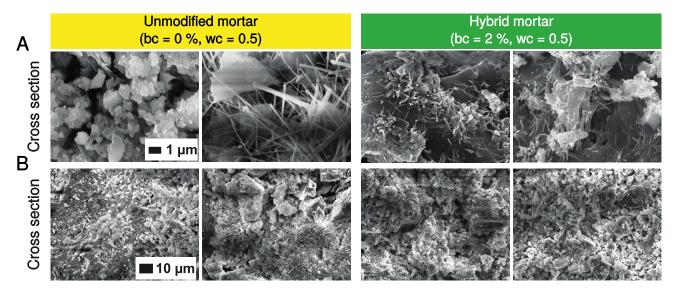
Figure 3.28: **SEM images of cross sections of unmodified and hybrid mortar samples:** Hybrid mortar samples show a higher density of ettringite-like crystals in the cross section than unmodified mortar samples. The 1 μm scale bar applies to all images in A, whereas the 10 μm scale bar applies to all images in B.

liquid suspension, the same wetting resistance was achieved compared to as when fresh biofilm was used (Fig. 3.27). This indeed renders the whole hybrid mortar casting process much simpler. Further experiments with this powder-based admixture revealed that even higher amounts of biofilm can be added to the mortar. Surprisingly, a hybrid mortar sample with a biofilm content of 10 % lyophilized biofilm powder can successfully be cast and, in contrast to the addition of fresh biofilm in the same amount, does not crumble. With this high amount of biofilm mass, the contact angle of the hybrid mortar samples even increased to ~110°, and sample-to-sample variations became much smaller than for the hybrid mortar samples supplemented with fresh biofilm (Fig. 3.27).

### 3.4.4 Water uptake of hybrid mortar

In the previous section, it was shown that the addition of biofilm, in either a fresh or a lyophilized state, leads to an increased wetting resistance of hybrid mortar. However, the increased wetting resistance was only determined directly after the water droplet was placed on the samples. In natural settings, water will reside for longer time spans on the mortar surface, or the mortar structure might even be submerged into water. Therefore, the contact angle for an unmodified mortar sample is, in a next step, compared with that of a hybrid mortar sample over prolonged time intervals. A water droplet placed onto an unmodified mortar sample is immediately soaked up by the material, whereas the contact angle on a hybrid mortar sample decreases slowly over time (Fig. 3.23A). Even after 60 minutes, the contact angle for the hybrid mortar samples is comparable with that of a PTFE sample (Fig. 3.23A).

However, in industrial settings, a high wetting resistance due to a surface modification may not be sufficient, since even a partial damage of the surface would lead to a loss of protection from water
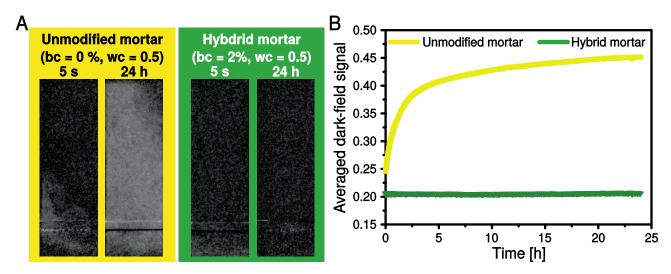
A



B



Figure 3.29: **Water uptake determined by X-ray dark-field imaging:** (A) X-ray dark-field radiographs at different time points (5 s and 24 h) for unmodified and hybrid mortar samples during capillary water uptake increasing from bottom to top. Brighter pixel values correspond to lower scattering strength, thus, higher water content. (B) Quantitative analysis of the time dependence of the water uptake. The average dark-field signal is shown for unmodified and hybrid mortar samples.

ingression. Therefore, it would be advantageous to achieve a delayed ingression of water by a bulk modification of the sample. This should be the case when the biofilm material is mixed with, and therefore distributed throughout, the mortar during the generation process. To check if the biofilm material is distributed well in the bulk material after the mortar casting process, hybrid mortar samples are cut and the cross section is visualized with SEM. The results show similar structures as already determined for the surface analysis with SEM: unmodified samples showed spike-like structures only in few spots whereas the hybrid mortar samples possessed a high density of these spike-like structures all over the surface (Fig. 3.28). These results demonstrate that indeed a bulk modification of the mortar structure is achieved, which in turn might increase the net surface of the inner material and thus the wetting energy. This leads to the notion that, in addition to the increased wetting resistance of the surface, the capillary uptake of water into the bulk material might be also delayed.

To test this idea, an experiment was designed to compare the water uptake by unmodified mortar with that of hybrid mortar. Mortar samples were prepared and the bottom of each of the samples was submerged into ddH$_2$O. X-ray dark field images of the samples were acquired during the experiment to determine the water ingression as a function of water exposure time. Directly after the start of the experiment, *i.e.* after 5 s, almost no water could be detected in either sample. After 24 h, however, the unmodified mortar sample was fully soaked with water. In contrast, in the hybrid mortar, no water could be detected even after this prolonged exposure time (Fig. 3.29A). When the averaged dark-field signal, which correlates with the total amount of water in the samples, is compared over time, the fast uptake of water into the unmodified mortar sample is clearly visible, whereas the hybrid mortar sample hardly takes up water at all. This verifies the hypothesis that the addition of biofilm to mortar delays the ingression of water into the hybrid mortar.

### 3.4.5 Discussion

In this chapter, the development and investigation of a hybrid mortar material with increased wetting resistance was described. This increased wetting resistance was achieved through the addition of biofilm formed by strain *B. subtilis* NCIB 3610 during the mortar generation process. It could be shown that the hydrophobic properties of the hybrid mortar are not based on the hydrophobicity of the biofilm itself, since also biofilm of hydrophilic nature induced a similar wetting resistance of the hybrid mortar. The increased wetting resistance is rather reached through a stimulation of mineralization processes during the hydration reaction of hybrid mortar. The increased density of spike-like crystal structures in the hybrid mortar is drastically increasing the roughness of the hybrid mortar samples. According to Wenzel (100), the contact angle of a rough surface $\Theta_r$ is calculated by $cos(\Theta_r)=rcos(\Theta)$, where $\Theta$ is the contact angle on an ideal flat surface and *r* the roughness ratio, which is defined as ratio of the true area of the solid surface to the apparent area. This increased surface area is the reason for the roughness-induced hydrophobicity of the mortar sample. The spike-like crystal structures can be found throughout the hybrid mortar material as determined by SEM. They seem to be part of the hydration reaction, as they were also found in unmodified mortar, however only at a few spots. These crystals could very well be ettringite-like crystals as they occur in standard Portland cement (96). A similar increase of the surface roughness of materials already has led to other artificial materials with extraordinary wetting resistance, *e.g.* slippery liquid-infused porous surfaces (101), and microstructured silicium surfaces (102).

However, the addition of fresh biofilm during the mortar generation process was limited to ~2.5%, because samples with a higher biofilm content crumbled easily and could not be successfully cast into a rigid form anymore. Surprisingly, if lyophilized biofilm was used for the hybrid mortar creation, it is possible to incorporate higher concentrations, *i.e.* 10 %, without the aforementioned effect of crumbling. One possible explanation for this different behavior could be that the freeze-drying process partly inactivates certain biofilm components which might be responsible for the crumbling of the hybrid mortar samples. Such an effect is in principle possible since protein degradation is known to occur for certain proteins during freeze-drying (103). However, such a destruction of biofilm components might not be likely since also the increased mineralization might be induced by proteins contained in the biofilm. Further, the virtually same wetting resistance is achieved for samples of 2 % biofilm content, for either fresh or lyophilized biofilm (Fig. 3.27).

One could also argue that with the addition of fresh biofilm to the mortar, extra water (contained in the highly hydrated fresh biofilm) is added and that this extra water alters the hydration reaction. It is known from standard mortar that additional water results in a more porous material, which could indeed lead to a mechanical unstable sample (104). However, the amount of additional water contained in the fresh biofilm is comparable to the water volume added when the wc is increased from 0.5 to 0.6 or 0.7. The biofilm mass added for a hybrid mortar sample with a biofilm content of 2 % is $m_{biofilm}$ = 0.8 g, and the amount of water contained in biofilm is usually in the range of 80-95 %. This would equal less than 1 mL of water, whereas an increase of the wc by 0.1 equals 1 mL of ddH$_2$O. Here, it was observed that even hybrid mortar samples with a wc of 0.7 can successfully be cast into a rigid form (Fig. 3.27).
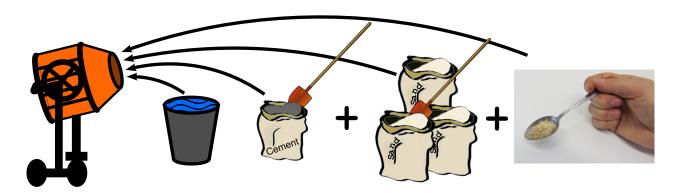
Figure 3.30: **Mixing of hybrid mortar:** Possible hybrid mortar generation process at a construction site, where cement, sand, water and lyophilized biofilm are simply mixed together.

The third, and most likely explanation why only up to 2.5 % of fresh biofilm can be added to the mortar are problems resulting from the mixing process. When fresh biofilm is added, cohesion forces in the biofilm could hamper a thorough distribution of the biofilm material in the mortar sample. Thus, local accumulations of biofilm material could locally provide higher amounts of water (contained in the biofilm chunks), resulting in a more porous and mechanical unstable structure of the hybrid mortar sample. When the biofilm material is freeze-dried prior to the mixing process, the distribution is probably much more homogeneous, allowing for the incorporation of 10 % lyophilized biofilm. Similar results have been observed for mineral admixtures to mortar where a higher fineness of the admixture correlates with an increased compression strength of mortar (105). Non biofilm-based approaches using other biological admixtures in cementitious materials to influence the material properties have gained attention in the past decade. The addition of biopolymers, bacteria, or bacterial cell walls for example lead to increased mechanical performance (106), protection of embedded steel structures from corrosion (107), and self-healing properties of cementitious materials (108).

The hybrid material presented here not only offers an increased wetting resistance over prolonged times, but also delays the ingression of water into the material by capillary forces when the samples are immersed into water. Since the biofilm material can be harvested and lyophilized prior to the casting process, the biofilm powder can be easily stored and added during the mixing process of mortar, *i.e.* at the construction site (Fig. 3.30). Thus, this approach is advantageous over post-curing surface modifications to achieve hydrophobicity (93, 94, 109): subsequent surface treatments are time-consuming and expensive compared to a simple admixture powder, since an additional working step has to be performed after mortar curing. Although such a simplicity in the mixing process can also be achieved with artificial admixtures, *e.g.* addition of waste paper sludge ash (110) or siloxane-based additives (111), those treatments may contain potentially harmful solvents. Thus, the hybrid mortar presented here may not only have a strong potential in industrial applications but is also eco-friendly as it only requires biological additives.

# Outlook

In this thesis, various material properties of bacterial biofilms were determined, and the influence of the matrix composition on these properties was investigated. Understanding these material properties is critically needed for the development of efficient biofilm removal and control strategies.

The erosion resistance of biofilms formed by the *B. subtilis* B-1 strain depends on the chemical environment the biofilm is exposed to. Metal ions which are present in the surrounding liquid are incorporated into the biofilm matrix. When ions are complexated by the polyanionic biopolymer γ-PGA, a main component of the B-1 biofilm matrix, a protection from erosion by fluid shear can be observed for selected metal ions. In some cases, this erosion protection is accompanied by a mechanical fortification of the biofilm matrix. However, it remains unclear why only selected metal ions induce such a change in erosion protection and/or the bulk viscoelasticity, since γ-PGA was reported to unselectively bind heavy metals (84). Further investigations on the role and influence of γ-PGA in the B-1 matrix are therefore necessary. Specifically, a knock-out mutant of strain B-1, unable to secret γ-PGA, could clarify whether this biopolymer is indeed responsible for the mechanical fortification of the biofilm matrix when exposed to metal ions.

Furthermore, experiments on the binding of purified γ-PGA to metal ions could clarify how the chelating agent EDTA competes with this biopolymer in terms of metal ion sequestering in the biofilm matrix. It was shown in this thesis, that the biofilm erosion protection induced by some metal ions could be countered by exposing the treated biofilms to an EDTA solution. To directly investigate if also a stiffening of the B-1 matrix, when treated with metal ions, can be counteracted by an ETDA solution, a submersion flow cell as presented in section 3.1.2 could be used. This setup enables the growth of biofilms *in situ* on the rheometer. The LB medium could then be changed to a solution containing metal ions and the time-dependent stiffening of the biofilm matrix could be observed. Afterwards, the metal ion solution could be replaced by an EDTA solution or other chelating agents. Since other chelating agents have different binding affinities to the metal ions tested, comparing the ensuing changes in viscoelasticity could then give insight into the binding affinity of metal ions to the biofilm matrix. Such experiments would be especially interesting for the previously mentioned γ-PGA knock-out B-1 strain. Furthermore, this method could be used with various bacterial species and corresponding knock-out strains to investigate the binding affinities of those biofilm matrices to metal ions. By varying the knocked-out biofilm components of each matrix, the matrix components responsible for viscoelastic stiffening could be identified.

Such a selective change in the mechanical behavior could be further investigated to develop a platform for the detection of certain metal ions in liquids. The detection and monitoring of metal ions is of great interest in many fields including molecular biology and environmental monitoring (112). Even though many approaches exist for sensing metal ions, they rely on the use of costly and difficult techniques *e.g.* atomic absorption spectroscopy (113) or inductively coupled plasma atomic emission spectrometry (114). Fluorescent based chemosensors represent a low-cost and simpler analytical method (115–117), yet, the detection of heavy metal ions such as $Fe^{3+}$ or $Cu^{2+}$ with such chemosensors is limited because these ions often act as fluorescent quenchers (118). A completely different detection method could be developed on the basis of a microfluidic device presented by Hohne *et. al* (65), which is able to determine the mechanical properties of soft viscoelastic materials grown on a membrane. The deflection of this membrane, induced by a defined pressure on the membrane, is a measure for the viscoelastic properties of the attached biofilm. A confocal laser scanning microscope was then used to determine the deflection. However, it might also be possible to measure this deflection with a resistance strain gauge in the future. This principle could be adapted to grow biofilm on the membrane and determine the viscoelastic properties of the biofilm. The test liquid could be flushed through the microfluidic channel so that the biofilm would be exposed to this liquid flow. If metal ions would be present in the test liquid, the biofilm matrix would stiffen, which in turn could be detected by the system. Since biofilms show different selectivity for metal ions (9, 10), different biofilms could be used to tune the abilities of this device. Finally, the mechanical fortification could be reversed by flushing the sensor with a chelating agent such as EDTA, which was found to wash metal ions out of the biofilm matrix (Sec. 3.1.2).

As biofilms are not only exposed to shear forces in their natural settings, further mechanical material properties need to be investigated to develop efficient biofilm removal strategies. The custom-built stretching device presented in this thesis is capable of measuring the tensile strength of biofilms grown *in situ*. Only few investigations were performed with this setup so far but it was shown that it is possible to measure the tensile strength of bacterial biofilms and that the influence of chemical treatments on the tensile strength can be investigated as well. It would also be interesting to see how other chemicals influence the tensile strength of the biofilm matrix of *B. subtilis* B-1, especially those used in the macrorheological assay performed in Section 3.1.3. With these measurements, the effect of the chemicals could then be determined for four different important material properties of $BF_{B-1}$. Yet, the treatment protocol used for samples in the stretching setup needs to be optimized, as the final concentration of the chemical in the biofilm remains unknown. Even though the concentration of the solution used for the chemical treatment is known, it is unclear how much of the chemical is actually absorbed into the biofilm matrix. An improvement could be achieved by using only low amounts of a chemical solution which can be fully soaked up by the biofilm matrix. However, a good distribution of such a small amount of liquid on the biofilm surface is difficult, since many biofilms exhibit strong hydrophobic properties and thus the biofilm surface could potentially not be wetted completely. Despite this strong hydrophobicity, it was shown in Section 3.1.2 that metal ions are able to penetrate the biofilm matrix. Therefore, investigations on the biofilm permeability for those chemicals could give insight on

how much ions are absorbed in the biofilm samples used for tensile testing.

The permeability of biofilms also plays an important role in the development of biofilm removal strategies. It was shown that even though biofilms are permeable for antibiotics, the antibiotics do not necessarily kill the embedded biofilm bacteria (119). A similar behavior was observed in this thesis when the biofilm was treated with potentially lethal metal ions (Sec. 3.1.5). One likely explanation for the protection of biofilm embedded bacteria is that toxic metal ions are trapped in the biofilm matrix. A reasonable strategy to kill biofilm embedded bacteria could therefore be to first target the molecules of the biofilm matrix responsible for ion trapping. Once these molecules are inactivated, the binding sites for the toxic substances would be missing in the biofilm matrix, thus allowing the toxic substances to reach and kill the embedded bacteria. Such a substance could be the γ-PGA hydrolase, which is able to degrade γ-PGA (120), and thus could be added prior to the viability assay presented in Section 3.1.5, to test whether γ-PGA is responsible for the binding of the metal ions and therefore protection of the embedded bacteria.

Even though biofilms constitute major problems in industrial settings, making use of their exceptional material properties could be interesting for technical applications. A new hybrid material was developed in this thesis by adding biofilm to a standard mortar mix. This hybrid material showed increased wetting resistance and delayed capillary uptake of water into the bulk material. However, it remains elusive whether the addition of the biofilm component changes other material properties of the hybrid mortar. It was observed that upon the addition of 3 % freshly harvested biofilm, the hybrid mortar samples crumbled easily. Even though higher amounts of biofilm could be added when the biofilm was lyophilized prior to its addition, this clearly indicates that the mechanical stability of the hybrid mortar might be compromised. Therefore, further investigations on the mechanical stability of hybrid mortar need to be performed. One important parameter for cementitious materials is the compression strength, which can easily be determined with commercially available standard testing equipment. In particular, the amount of biofilm added may correlate with a decrease in compression strength of the hybrid mortar samples. The workability and reaction kinetics of the hydration reaction of the hybrid mortar mix could be analyzed with a rheometer, whereas 3-point bending tests may give insight into the fracture toughness of the hybrid material. In general, all specifications as defined in the European Norm EN 998-1 must be met before an industrial application is possible.

Furthermore, to render the hybrid mortar material more suitable for an industry-scaled production, the harvesting of the biofilm needs to be simplified and automated. This could be achieved when biofilms are grown at the air-liquid interphase where they form so-called pellicles. Even though this approach has not been tested in this thesis, it is likely that such a pellicle would induce comparable results when added to mortar as the structure and composition of floating pellicles seems to be similar to that of biofilms formed on a solid nutrition layer (2). Such pellicles could then be grown in a liquid culture which is constantly replenished with nutrients, and harvested through an automated process which siphons the biofilm pellicles off the liquid surface for further processing. This further processing could include an automatic freeze-drying of the skimmed biomaterial. However, since freeze-drying is a rather expensive process (121), a simple drying of the biofilm material might be sufficient. Further

tests on the laboratory scale could examine the applicability of those methods for the scale-up of the hybrid mortar production.

# Bibliography

[1] L. Hall-Stoodley, J. W. Costerton, and P. Stoodley, Bacterial biofilms: from the natural environment to infectious diseases, *Nat Rev Micro*, vol. 2, no. 2, p. 95–108, 2004.

[2] S. Branda, F. Chu, D. Kearns, R. Losick, and R. Kolter, A major protein component of the *Bacillus subtilis* biofilm matrix, *Mol Microbiol*, vol. 59, no. 4, pp. 1229–1238, 2006.

[3] H.-C. Flemming and J. Wingender, The biofilm matrix, *Nat Rev Microbiol*, vol. 8, no. 9, pp. 623–633, 2010.

[4] K. P. Lemon, A. M. Earl, H. C. Vlamakis, C. Aguilar, and R. Kolter, Biofilm development with an emphasis on *Bacillus subtilis*, in *Bacterial Biofilms*, ser. Current topics in microbiology and immunology, Springer-Verlag Berlin, vol. 322, pp. 1–16.

[5] M. Marvasi, P. T. Visscher, and L. C. Martinez, Exopolymeric substances (eps) from *Bacillus subtilis*: polymers and genes encoding their synthesis, *FEMS Microbiol Lett*, vol. 313, no. 1, pp. 1–9, 2010.

[6] A. K. Epstein, B. Pokroy, A. Seminara, and J. Aizenberg, Bacterial biofilm shows persistent resistance to liquid wetting and gas penetration, *Proc Natl Acad Sci USA*, vol. 108, no. 3, pp. 995–1000, 2011.

[7] J. Costerton, P. Stewart, and E. Greenberg, Bacterial biofilms: A common cause of persistent infections, *Science*, vol. 284, no. 5418, pp. 1318–1322, 1999.

[8] R. Singh, P. Ray, A. Das, and M. Sharma, Penetration of antibiotics through *Staphylococcus aureus* and *Staphylococcus epidermidis* biofilms, *J Antimicrob Chemother*, vol. 65, no. 9, pp. 1955–1958, 2010.

[9] O. Lieleg, M. Caldara, R. Baumgaertel, and K. Ribbeck, Mechanical robustness of *Pseudomonas aeruginosa* biofilms, *Soft Matter*, vol. 7, no. 7, pp. 3307–3314, 2011.

[10] S. Grumbein, M. Opitz, and O. Lieleg, Selected metal ions protect *Bacillus subtilis* biofilms from erosion, *Metallomics*, vol. 6, no. 8, p. 1441, 2014.

[11] A.-L. Reysenbach and S. L. Cady, Microbiology of ancient and modern hydrothermal systems, *Trends in Microbiology*, vol. 9, no. 2, p. 79–86, 2001.

[12] C. D. Taylor, C. O. Wirsen, and F. Gaill, Rapid microbial production of filamentous sulfur mats at hydrothermal vents, *Appl Environ Microbiol*, vol. 65, no. 5, pp. 2253–2255, 1999.

[13] M. Morikawa, Beneficial biofilm formation by industrial bacteria *Bacillus subtilis* and related species, *J Biosci Bioeng*, vol. 101, no. 1, pp. 1–8, 2006.

[14] S. S. Socransky and A. D. Haffajee, Dental biofilms: difficult therapeutic targets, *Periodontology 2000*, vol. 28, no. 1, p. 12–55, 2002.

[15] B. W. Trautner and R. O. Darouiche, Role of biofilm in catheter-associated urinary tract infection , *American Journal of Infection Control*, vol. 32, no. 3, p. 177–183, 2004.

[16] J. C. Block, K. Haudidier, J. L. Paquin, J. Miazga, and Y. Levi, Biofilm accumulation in drinking water distribution systems, *Biofouling*, vol. 6, no. 4, p. 333–343, 1993.

[17] R. M. Donlan, Biofilms: Microbial life on surfaces, *Emerging Infectious Diseases*, vol. 8, no. 9, pp. 881–890, 2002.

[18] H.-C. Flemming, Biofouling in water systems – cases, causes and countermeasures, *Applied Microbiology and Biotechnology*, vol. 59, no. 6, pp. 629–640, 2002.

[19] T. E. Cloete, Biofouling control in industrial water systems: What we know and what we need to know, *Materials and Corrosion*, vol. 54, no. 7, p. 520–526, 2003.

[20] W. Costerton, R. Veeh, M. Shirtliff, M. Pasmore, C. Post, and G. Ehrlich, The application of biofilm science to the study and control of chronic bacterial infections, *J. Clin. Invest.*, vol. 112, no. 10, p. 1466–1477, 2003.

[21] L. Pavlovsky, R. A. Sturtevant, J. G. Younger, and M. J. Solomon, Effects of temperature on the morphological, polymeric, and mechanical properties of *Staphylococcus epidermidis* bacterial biofilms, *Langmuir*, vol. 31, no. 6, p. 2036–2042, 2015.

[22] J. K. Teschler, D. Zamorano-Sánchez, A. S. Utada, C. J. A. Warner, G. C. L. Wong, R. G. Linington, and F. H. Yildiz, Living in the matrix: assembly and control of *Vibrio cholerae* biofilms, *Nat Rev Micro*, vol. 13, no. 5, p. 255–268, 2015.

[23] L. S. Cairns, L. Hobley, and N. R. Stanley-Wall, Biofilm formation by *Bacillus subtilis*: new insights into regulatory strategies and assembly mechanisms, *Molecular Microbiology*, vol. 93, no. 4, p. 587–598, 2014.

[24] E. Hollenbeck, J. Fong, J. Lim, F. Yildiz, G. Fuller, and L. Cegelski, Molecular determinants of mechanical properties of *V. cholerae* biofilms at the air-liquid interface, *Biophysical Journal*, vol. 107, no. 10, p. 2245–2252, 2014.

[25] W. Zhang, W. Dai, S.-M. Tsai, S. M. Zehnder, M. Sarntinoranont, and T. E. Angelini, Surface indentation and fluid intake generated by the polymer matrix of *Bacillus subtilis* biofilms, *Soft Matter*, vol. 11, no. 18, p. 3612–3617, 2015.

[26] M. Hentzer, G. M. Teitzel, G. J. Balzer, A. Heydorn, S. Molin, M. Givskov, and M. R. Parsek, Alginate overproduction affects *Pseudomonas aeruginosa* biofilm structure and function, *Journal of Bacteriology*, vol. 183, no. 18, p. 5395–5401, 2001.

[27] E. E. Mann and D. J. Wozniak, *Pseudomonas* biofilm matrix composition and niche biology, *FEMS Microbiol Rev*, vol. 36, no. 4, p. 893–916, 2012.

[28] Y. Asahi, J. Miura, T. Tsuda, S. Kuwabata, K. Tsunashima, Y. Noiri, T. Sakata, S. Ebisu, and M. Hayashi, Simple observation of *Streptococcus mutans* biofilm by scanning electron microscopy using ionic liquids, *AMB Express*, vol. 5, no. 1, 2015.

[29] V. Lazarova, Biofilm characterization and activity analysis in water and wastewater treatment, *Water Research*, vol. 29, no. 10, p. 2227–2245, 1995.

[30] R. Singh, D. Paul, and R. K. Jain, Biofilms: implications in bioremediation, *Trends in Microbiology*, vol. 14, no. 9, p. 389–397, 2006.

[31] L. Westers, H. Westers, and W. J. Quax, *Bacillus subtilis* as cell factory for pharmaceutical proteins: a biotechnological approach to optimize the host organism, *Biochimica et Biophysica Acta (BBA) - Molecular Cell Research*, vol. 1694, no. 1-3, p. 299–310, 2004.

[32] J. C. Zweers, I. Barák, D. Becher, A. J. Driessen, M. Hecker, V. P. Kontinen, M. J. Saller, L. Vavrová, and J. van Dijl, Towards the development of *Bacillus subtilis* as a cell factory for membrane proteins and protein complexes, *Microbial Cell Factories*, vol. 7, no. 1, p. 10, 2008.

[33] S. Kesel, S. Grumbein, I. Gümperlein, M. Tallawi, A.-K. Marel, O. Lieleg, and M. Opitz, Direct comparison of physical properties of *Bacillus subtilis* NCIB 3610 and B-1 biofilms, *Appl. Environ. Microbiol.*, p. AEM.03957–15, 2016.

[34] M. Morikawa, S. Kagihiro, M. Haruki, K. Takano, S. Branda, R. Kolter, and S. Kanaya, Biofilm formation by a *Bacillus subtilis* strain that produces gamma-polyglutamate. *Microbiology*, vol. 152, no. Pt 9, pp. 2801–2807, 2006.

[35] S. S. Branda, J. E. González-Pastor, S. Ben-Yehuda, R. Losick, and R. Kolter, Fruiting body formation by *Bacillus subtilis*. *Proc Natl Acad Sci U S A*, vol. 98, no. 20, pp. 11 621–11 626, 2001.

[36] H. Vlamakis, C. Aguilar, R. Losick, and R. Kolter, Control of cell fate by the formation of an architecturally complex bacterial community. *Genes Dev*, vol. 22, no. 7, pp. 945–953, 2008.

[37] K. Kobayashi and M. Iwano, Bsla(yuab) forms a hydrophobic layer on the surface of *Bacillus subtilis* biofilms. *Mol Microbiol*, vol. 85, no. 1, pp. 51–66, 2012.

[38] Y. Chai, P. B. Beauregard, H. Vlamakis, R. Losick, and R. Kolter, Galactose metabolism plays a crucial role in biofilm formation by *Bacillus subtilis*. *MBio*, vol. 3, no. 4, pp. e00 184–e00 112, 2012.

[39] J. N. Wilking, T. E. Angelini, A. Seminara, M. P. Brenner, and D. A. Weitz, Biofilms as complex fluids, *MRS Bulletin*, vol. 36, no. 5, pp. 385–391, 2011.

[40] O. Lieleg, Model systems of the actin cortex, Dissertation, Technische Universität München, München, 2008.

[41] T. G. Kuznetsova, M. N. Starodubtseva, N. I. Yegorenkov, S. A. Chizhik, and R. I. Zhdanov, Atomic force microscopy probing of cell elasticity, *Micron*, vol. 38, no. 8, p. 824–833, 2007.

[42] A. Stalder, G. Kulik, D. Sage, L. Barbieri, and P. Hoffmann, A snake-based approach to accurate determination of both contact points and contact angles, *Colloids and Surfaces A: Physicochemical and Engineering Aspects*, vol. 286, no. 1-3, p. 92–103, 2006.

[43] F. Prade, M. Chabior, F. Malm, C. Grosse, and F. Pfeiffer, Observing the setting and hardening of cementitious materials by X-ray dark-field radiography, *Cement and Concrete Research*, vol. 74, p. 19–25, 2015.

[44] K. Bundy, Measurement of fibroblast and bacterial detachment from biomaterials using jet impingement, *Cell Biology International*, vol. 25, no. 4, p. 289–307, 2001.

[45] S. Bayoudh, L. Ponsonnet, H. B. Ouada, A. Bakhrouf, and A. Othmane, Bacterial detachment from hydrophilic and hydrophobic surfaces using a microjet impingement, *Colloids and Surfaces A: Physicochemical and Engineering Aspects*, vol. 266, no. 1-3, p. 160–167, 2005.

[46] C. Coufort, N. Derlon, J. Ochoa-Chaves, A. Liné, and E. Paul, Cohesion and detachment in biofilm systems for different electron acceptor and donors, *Water Science & Technology*, vol. 55, no. 8-9, p. 421, 2007.

[47] M. Simões, M. Pereira, and M. Vieira, Effect of mechanical stress on biofilms challenged by different chemicals, *Water Res*, vol. 39, no. 20, pp. 5142–5152, 2005.

[48] J. Kreth, E. Hagerman, K. Tam, J. Merritt, D. T. W. Wong, B. M. Wu, N. V. Myung, W. Shi, and F. Qi, Quantitative analyses of *Streptococcus mutans* biofilms with quartz crystal microbalance, microjet impingement and confocal microscopy, *Biofilms*, vol. 1, no. 4, p. 277–284, 1999.

[49] B. N. Clark, S. V. Masters, and M. A. Edwards, Lead release to drinking water from galvanized steel pipe coatings, *Environmental Engineering Science*, vol. 32, no. 8, p. 713–721, 2015.

[50] S. C. Andrews, A. K. Robinson, and F. Rodríguez-Quiñones, Bacterial iron homeostasis, *FEMS Microbiol Rev*, vol. 27, no. 2-3, pp. 215–237, 2003.

[51] T. Bjarnsholt, The role of bacterial biofilms in chronic infections, *APMIS*, vol. 121, pp. 1–58, 2013.

[52] P. S. Stewart, Theoretical aspects of antibiotic diffusion into microbial biofilms. *Antimicrob Agents Chemother*, vol. 40, no. 11, pp. 2517–2522, 1996.

[53] P. Stoodley, R. Cargo, C. Rupp, S. Wilson, and I. Klapper, Biofilm material properties as related to shear-induced deformation and detachment phenomena, *J Ind Microbiol*, vol. 29, no. 6, pp. 361–367, 2002.

[54] P. Sarin, V. Snoeyink, J. Bebee, K. Jim, M. Beckett, W. Kriven, and J. Clement, Iron release from corroded iron pipes in drinking water distribution systems: effect of dissolved oxygen, *Water Research*, vol. 38, no. 5, p. 1259–1269, 2004.

[55] V. Körstgens, H. C. Flemming, J. Wingender, and W. Borchard, Influence of calcium ions on the mechanical properties of a model biofilm of mucoid *Pseudomonas aeruginosa*. *Water Sci Technol*, vol. 43, no. 6, pp. 49–57, 2001.

[56] L. C. Simões, M. Lemos, P. Araújo, A. M. Pereira, and M. Simões, The effects of glutaraldehyde on the control of single and dual biofilms of *Bacillus cereus* and *Pseudomonas fluorescens*, *Biofouling*, vol. 27, no. 3, pp. 337–346, 2011.

[57] E. R. Brindle, D. A. Miller, and P. S. Stewart, Hydrodynamic deformation and removal of *Staphylococcus epidermidis* biofilms treated with urea, chlorhexidine, iron chloride, or dispersinb, *Biotechnol Bioeng*, vol. 108, no. 12, pp. 2968–2977, 2011.

[58] G. M. Teitzel and M. R. Parsek, Heavy metal resistance of biofilm and planktonic *Pseudomonas aeruginosa*, *Applied and Environmental Microbiology*, vol. 69, no. 4, p. 2313–2320, 2003.

[59] S. Langley and T. J. Beveridge, Metal binding by *Pseudomonas aeruginosa* PAO1 is influenced by growth of the cells as a biofilm, *Canadian Journal of Microbiology*, vol. 45, no. 7, p. 616–622, 1999.

[60] J. J. Harrison, H. Ceri, and R. J. Turner, Multimetal resistance and tolerance in microbial biofilms, *Nat Rev Microbiol*, vol. 5, no. 12, pp. 928–938, 2007.

[61] D. Sun, S. Roth, and M. J. Black, Secrets of optical flow estimation and their principles, *2010 IEEE Computer Society Conference on Computer Vision and Pattern Recognition*, 2010.

[62] S. Aggarwal and R. M. Hozalski, Effect of strain rate on the mechanical properties of *Staphylococcus epidermidis* biofilms, *Langmuir*, vol. 28, no. 5, pp. 2812–2816, 2012.

[63] E. Vignaga, H. Haynes, and W. Sloan, Quantifying the tensile strength of microbial mats grown over noncohesive sediments, *Biotechnology and Bioengineering*, vol. 109, no. 5, pp. 1155–1164, 2012.

[64] G. Bell, Models for the specific adhesion of cells to cells, *Science*, vol. 200, no. 4342, p. 618–627, 1978.

[65] D. N. Hohne, J. G. Younger, and M. J. Solomon, Flexible microfluidic device for mechanical property characterization of soft viscoelastic solids such as bacterial biofilms, *Langmuir*, vol. 25, no. 13, pp. 7743–7751, 2009.

[66] L. Pavlovsky, J. G. Younger, and M. J. Solomon, In situ rheology of *Staphylococcus epidermidis* bacterial biofilms, *Soft Matter*, vol. 9, no. 1, pp. 122–131, 2013.

[67] S. S. Rogers, C. van der Walle, and T. A. Waigh, Microrheology of bacterial biofilms in vitro: *Staphylococcus aureus* and *Pseudomonas aeruginosa*, *Langmuir*, vol. 24, no. 23, pp. 13 549–13 555, 2008.

[68] A. Ohashi, T. Koyama, K. Syutsubo, and H. Harada, A novel method for evaluation of biofilm tensile strength resisting erosion, *Water Science and Technology*, vol. 39, no. 7, p. 261–268, 1999.

[69] A. W. Cense, E. A. G. Peeters, B. Gottenbos, F. P. T. Baaijem, A. M. Nuijs, and M. E. H. van Dongen, Mechanical properties and failure of *Streptococcus mutans* biofilms, studied using a microindentation device, *J Microbiol Methods*, vol. 67, no. 3, pp. 463–472, 2006.

[70] S. Aggarwal, E. H. Poppele, and R. M. Hozalski, Development and testing of a novel micro-cantilever technique for measuring the cohesive strength of intact biofilms, *Biotechnology and Bioengineering*, pp. 924–934, 2010.

[71] E. H. Poppele and R. M. Hozalski, Micro-cantilever method for measuring the tensile strength of biofilms and microbial flocs, *Journal of Microbiological Methods*, vol. 55, no. 3, pp. 607 – 615, 2003.

[72] P. Stoodley, L. Hall-Stoodley, and H. Lappin-Scott, Detachment, surface migration, and other dynamic behavior in bacterial biofilms revealed by digital time-lapse imaging, in *Microbial Growth In Biofilms, Pt B*, ser. Methods in Enzymology, Academic Press Inc., vol. 337, pp. 306–318.

[73] E. Banin, K. M. Brady, and E. P. Greenberg, Chelator-induced dispersal and killing of *Pseudomonas aeruginosa* cells in a biofilm, *Appl Environ Microbiol*, vol. 72, no. 3, pp. 2064–2069, 2006.

[74] W. L. Jones, M. P. Sutton, L. McKittrick, and P. S. Stewart, Chemical and antimicrobial treatments change the viscoelastic properties of bacterial biofilms, *Biofouling*, vol. 27, no. 2, pp. 207–215, 2011.

[75] H. Vlamakis, Y. Chai, P. Beauregard, R. Losick, and R. Kolter, Sticking together: building a biofilm the *Bacillus subtilis* way, *Nat Rev Micro*, vol. 11, no. 3, p. 157–168, 2013.

[76] S. Kesel, F. Moormann, I. Gumperlein, A. Mader, M. Morikawa, O. Lieleg, and M. Opitz, Draft genome sequence of the biofilm-producing *Bacillus subtilis* strain B-1, isolated from an oil field, *Genome Announcements*, vol. 2, no. 6, p. e01163–14–e01163–14, 2014.

[77] D. Romero, C. Aguilar, R. Losick, and R. Kolter, Amyloid fibers provide structural integrity to *Bacillus subtilis* biofilms, *Proc Natl Acad Sci USA*, vol. 107, no. 5, pp. 2230–2234, 2010.

[78] L. Hobley, A. Ostrowski, F. V. Rao, K. M. Bromley, M. Porter, A. R. Prescott, C. E. MacPhee, D. M. F. van Aalten, and N. R. Stanley-Wall, Bsla is a self-assembling bacterial hydrophobin that coats the *Bacillus subtilis* biofilm, *Proceedings of the National Academy of Sciences*, vol. 110, no. 33, p. 13600–13605, 2013.

[79] H. Haga, S. Sasaki, M. Morimoto, K. Kawabata, E. Ito, K. Abe, and T. Sambongi, Imaging elastic properties of soft materials immersed in water using force modulation mode in atomic force microscopy, *Japanese Journal of Applied Physics*, vol. 37, no. Part 1, No. 6B, p. 3860–3863, 1998.

[80] A. Ostrowski, A. Mehert, A. Prescott, T. B. Kiley, and N. R. Stanley-Wall, Yuab functions synergistically with the exopolysaccharide and tasa amyloid fibers to allow biofilm formation by *Bacillus subtilis*, *Journal of Bacteriology*, vol. 193, no. 18, p. 4821–4831, 2011.

[81] A. Steinbüchel, C. Ewering, F. Oppermann-Sanio, M. Pötter, and F. Reinecke, *Mikrobiologisches Praktikum: Versuche und Theorie*, ser. Springer-Lehrbuch, Springer Berlin Heidelberg.

[82] I.-L. Shih and Y.-T. Van, The production of poly-(γ-glutamic acid) from microorganisms and its various applications, *Bioresource Technology*, vol. 79, no. 3, p. 207–225, 2001.

[83] T. Candela and A. Fouet, Poly-gamma-glutamate in bacteria, *Mol Microbiol*, vol. 60, no. 5, p. 1091–1098, 2006.

[84] R. J. C. McLean, D. Beauchemin, L. Clapham, and T. J. Beveridge, Metal-binding characteristics of the gamma-glutamyl capsular polymer of *Bacillus licheniformis* ATCC 9945, *Appl. Environ. Microbiol.*, vol. 56, no. 12, pp. 3671–3677, 1990.

[85] B. Bhushan and M. Nosonovsky, The rose petal effect and the modes of superhydrophobicity, *Philosophical Transactions of the Royal Society A: Mathematical, Physical and Engineering Sciences*, vol. 368, no. 1929, p. 4713–4728, 2010.

[86] R. Blossey, Self-cleaning surfaces — virtual realities, *Nat Mater*, vol. 2, no. 5, p. 301–306, 2003.

[87] A. K. Epstein, T.-S. Wong, R. A. Belisle, E. M. Boggs, and J. Aizenberg, Liquid-infused structured surfaces with exceptional anti-biofouling performance, *Proc Natl Acad Sci USA*, vol. 109, no. 33, pp. 13 182–13 187, 2012.

[88] A. Gauthier, S. Symon, C. Clanet, and D. Quéré, Water impacting on superhydrophobic macro-textures, *Nat Comms*, vol. 6, p. 8001, 2015.

[89] E. Celia, T. Darmanin, E. Taffin de Givenchy, S. Amigoni, and F. Guittard, Recent advances in designing superhydrophobic surfaces, *Journal of Colloid and Interface Science*, vol. 402, p. 1–18, 2013.

[90] M. Wu, B. Ma, T. Pan, S. Chen, and J. Sun, Silver-nanoparticle-colored cotton fabrics with tunable colors and durable antibacterial and self-healing superhydrophobic properties, *Advanced Functional Materials*, vol. 26, no. 4, p. 569–576, 2015.

[91] J. E. Mates, I. S. Bayer, J. M. Palumbo, P. J. Carroll, and C. M. Megaridis, Extremely stretchable and conductive water-repellent coatings for low-cost ultra-flexible electronics, *Nat Comms*, vol. 6, p. 8874, 2015.

[92] S. Ahmad, Reinforcement corrosion in concrete structures, its monitoring and service life prediction—a review, *Cement and Concrete Composites*, vol. 25, no. 4-5, p. 459–471, 2003.

[93] I. Flores-Vivian, V. Hejazi, M. I. Kozhukhova, M. Nosonovsky, and K. Sobolev, Self-assembling particle-siloxane coatings for superhydrophobic concrete, *ACS Applied Materials & Interfaces*, vol. 5, no. 24, p. 13284–13294, 2013.

[94] D. Barnat-Hunek and P. Smarzewski, Influence of hydrophobisation on surface free energy of hybrid fiber reinforced ultra-high performance concrete, *Construction and Building Materials*, vol. 102, p. 367–377, 2016.

[95] M. Shemesh and Y. Chai, A combination of glycerol and manganese promotes biofilm formation in *Bacillus subtilis* via histidine kinase kind signaling, *Journal of Bacteriology*, vol. 195, no. 12, p. 2747–2754, 2013.

[96] H. E. Schwiete and E. M. G. Niel, Formation of ettringite immediately after gaging of a portland cement, *J American Ceramic Society*, vol. 48, no. 1, p. 12–14, 1965.

[97] V. G. Haach, G. Vasconcelos, and P. B. Lourenço, Influence of aggregates grading and water/cement ratio in workability and hardened properties of mortars, *Construction and Building Materials*, vol. 25, no. 6, p. 2980–2987, 2011.

[98] G. Rao, Generalization of abrams' law for cement mortars, *Cement and Concrete Research*, vol. 31, no. 3, p. 495–502, 2001.

[99] O. Jensen, P. Hansen, A. Coats, and F. Glasser, Chloride ingress in cement paste and mortar, *Cement and Concrete Research*, vol. 29, no. 9, p. 1497–1504, 1999.

[100] R. N. Wenzel, Resistance of solid surfaces to wetting by water, *Industrial & Engineering Chemistry*, vol. 28, no. 8, p. 988–994, 1936.

[101] T.-S. Wong, S. H. Kang, S. K. Y. Tang, E. J. Smythe, B. D. Hatton, A. Grinthal, and J. Aizenberg, Bioinspired self-repairing slippery surfaces with pressure-stable omniphobicity, *Nature*, vol. 477, no. 7365, p. 443–447, 2011.

[102] B. Bhushan and E. K. Her, Fabrication of superhydrophobic surfaces with high and low adhesion inspired from rose petal, *Langmuir*, vol. 26, no. 11, p. 8207–8217, 2010.

[103] I. Roy and M. Gupta, Freeze-drying of proteins: some emerging concerns, *Biotechnology and Applied Biochemistry*, vol. 39, no. 2, p. 165, 2004.

[104] F. H. Wittmann, P. E. Roelfstra, H. Mihashi, Y.-Y. Huang, X.-H. Zhang, and N. Nomura, Influence of age of loading, water-cement ratio and rate of loading on fracture energy of concrete, *Materials and Structures*, vol. 20, no. 2, pp. 103–110, 1987.

[105] P. Lawrence, M. Cyr, and E. Ringot, Mineral admixtures in mortars effect of type, amount and fineness of fine constituents on compressive strength, *Cement and Concrete Research*, vol. 35, no. 6, p. 1092–1105, 2005.

[106] R. Pei, J. Liu, S. Wang, and M. Yang, Use of bacterial cell walls to improve the mechanical performance of concrete, *Cement and Concrete Composites*, vol. 39, p. 122–130, 2013.

[107] S. Roux, N. Bur, G. Ferrari, B. Tribollet, and F. Feugeas, Influence of a biopolymer admixture on corrosion behaviour of steel rebars in concrete, *Materials and Corrosion*, vol. 61, no. 12, p. 1026–1033, 2010.

[108] H. M. Jonkers, *Self Healing Materials: An Alternative Approach to 20 Centuries of Materials Science*, Springer Netherlands, ch. Self Healing Concrete: A Biological Approach, pp. 195–204.

[109] R. Ramachandran, K. Sobolev, and M. Nosonovsky, Dynamics of droplet impact on hydrophobic/icephobic concrete with the potential for superhydrophobicity, *Langmuir*, vol. 31, no. 4, p. 1437–1444, 2015.

[110] H. S. Wong, R. Barakat, A. Alhilali, M. Saleh, and C. R. Cheeseman, Hydrophobic concrete using waste paper sludge ash, *Cement and Concrete Research*, vol. 70, p. 9–20, 2015.

[111] S. Muzenski, I. Flores-Vivian, and K. Sobolev, Durability of superhydrophobic engineered cementitious composites, *Construction and Building Materials*, vol. 81, p. 291–297, 2015.

[112] Y. Choi, Y. Park, T. Kang, and L. P. Lee, Selective and sensitive detection of metal ions by plasmonic resonance energy transfer-based nanospectroscopy, *Nature Nanotechnology*, vol. 4, no. 11, p. 742–746, 2009.

[113] O. T. Butler, J. M. Cook, C. F. Harrington, S. J. Hill, J. Rieuwerts, and D. L. Miles, Atomic spectrometry update. environmental analysis, *J. Anal. At. Spectrom.*, vol. 21, no. 2, p. 217–243, 2006.

[114] Y. Li, C. Chen, B. Li, J. Sun, J. Wang, Y. Gao, Y. Zhao, and Z. Chai, Elimination efficiency of different reagents for the memory effect of mercury using ICp-ms, *J. Anal. At. Spectrom.*, vol. 21, no. 1, p. 94–96, 2006.

[115] H. Szmacinski, I. Gryczynski, and J. R. Lakowicz, Calcium-dependent fluorescence lifetimes of indo-1 for one- and two-photon excitation of fluorescence, *Photochem Photobiol*, vol. 58, no. 3, p. 341–345, 1993.

[116] A. K. Yetisen, Y. Montelongo, M. M. Qasim, H. Butt, T. D. Wilkinson, M. J. Monteiro, and S. H. Yun, Photonic nanosensor for colorimetric detection of metal ions, *Anal. Chem.*, vol. 87, no. 10, p. 5101–5108, 2015.

[117] M. Leermakers, W. Baeyens, P. Quevauviller, and M. Horvat, Mercury in environmental samples: Speciation, artifacts and validation, *TrAC Trends in Analytical Chemistry*, vol. 24, no. 5, p. 383–393, 2005.

[118] D. T. Quang and J. S. Kim, Fluoro- and chromogenic chemodosimeters for heavy metal ion detection in solution and biospecimens, *Chem. Rev.*, vol. 110, no. 10, p. 6280–6301, 2010.

[119] J. N. Anderl, M. J. Franklin, and P. S. Stewart, Role of antibiotic penetration limitation in *Klebsiella pneumoniae* biofilm resistance to ampicillin and ciprofloxacin, *Antimicrobial Agents and Chemotherapy*, vol. 44, no. 7, p. 1818–1824, 2000.

[120] S. Mamberti, P. Prati, P. Cremaschi, C. Seppi, C. F. Morelli, A. Galizzi, M. Fabbi, and C. Calvio, γ-pga hydrolases of phage origin in *Bacillus subtilis* and other microbial genomes, *PLoS ONE*, vol. 10, no. 7, p. e0130810, 2015.

[121] C. Ratti, Hot air and freeze-drying of high-value foods: a review, *Journal of Food Engineering*, vol. 49, no. 4, p. 311–319, 2001.

# Acknowledgements

# Publikationsliste

**S. Grumbein**, M. Opitz and O. Lieleg,
Selected metal ions protect *Bacillus subtilis* biofilms from erosion,
*Metallomics* **8**(6), 1441-1450 (2014)


K. Boettcher, **S. Grumbein**, U. Winkler, J. Nachtsheim, M. Opitz and O. Lieleg,
Adapting a commercial shear rheometer for applications in cartilage research,
*Review of Scientific Instruments* **9**(85), 093903 (2014)


S. Kesel*, **S. Grumbein***, I. Gümperlein, M. Tallawi, AK. Marel, O. Lieleg and M. Opitz,
Direct comparison of physical properties of *Bacillus subtilis* NCIB 3610 and B-1 biofilms,
*Appl. Environ. Microbiol.*, **82**(8), 2424-2432 (2016)


**S. Grumbein**, M. Werb, M. Opitz, and O. Lieleg,
Elongational rheology of bacterial biofilms *in situ*
*Journal of Rheology*, **60**(6), 1085-1094 (2016)


**S. Grumbein***, D. Minev*, M. Tallawi*, K. Boettcher, F. Prade, F. Pfeiffer, C.U. Grosse, and O. Lieleg,
Hydrophobic properties of biofilm-enriched hybrid mortar
*Advanced Materials*, **28**(37), 8138-8143 (2016)